

PETROLOGY OF SILICATE INCLUSIONS IN THE MILES IIE IRON

Yukio IKEDA¹ and Martin PRINZ²

¹*Department of Earth Sciences, Ibaraki University, Mito 310*

²*Department of Earth and Planetary Sciences, American Museum of Natural History,
New York, NY 10024, U.S.A.*

Abstract: The Miles IIE iron contains many silicate inclusions with gabbroic and cryptocrystalline textures. The gabbroic inclusions consist of inverted pigeonite, orthopyroxene, high-Ca pyroxene, olivine, sodic plagioclase, antiperthite, K-feldspar, tridymite, granitic glass, chromite, rutile, armalcolite, ilmenite, whitlockite, chlorapatite, troilite, schreibersite, taenite, and kamacite. They are the crystallization products of silicate melts which were produced by equilibrium or impact partial melting of an H chondritic precursor, and the degree of melting was variable, but about 25% on the average. Partial melting probably took place in a regolithic breccia on an H chondritic parent body. The melts experienced reduction during their crystallization. The cryptocrystalline inclusions consist mainly of cryptocrystalline albite and alkali feldspar, and sometimes have phenocrystic clinopyroxene, needles of orthopyroxene, and/or whitlockite-predominant nodules. Some nodules include P-bearing magnesian olivine, sodalite, and rutile, and these nodules appear to have separated as P₂O₅-rich melts from the albite-rich melt by liquid immiscibility. The inclusions cooled rapidly, resulting in their cryptocrystalline textures.

1. Introduction

Miles is a IIE iron found in 1992 in Queensland, Australia, and the total mass is about 265 kg (WLOTZKA, 1994). It contains many silicate inclusions, and the volume of the silicate inclusions appears to be about 10–20%.

Because silicates in IIE irons have oxygen isotopic compositions similar to those of H chondrites (RUBIN *et al.*, 1986; MAYEDA and CLAYTON, 1989), these two groups may have an intimate genetic relationship, and were probably produced in an H chondritic body(ies) (WASSON and WANG, 1986). There are two major hypotheses for the origin of silicate inclusions in IIE irons. One is a near-surface model in which IIE irons with silicates were produced at the surface, or in a shallow zone, of (an) H chondritic parent body(ies) (WASSON and WANG, 1986; OLSEN *et al.*, 1994; CASANOVA *et al.*, 1995). An alternative model is a core-mantle hypothesis in which the IIE irons with silicates were produced by the mixing of metallic melts and silicates in a core-mantle environment of the chondritic parent body(ies) (McCOY, 1995).

IIE silicate inclusions are variable in their compositions and textures among the IIE meteorites, and they have been classified into two types, unfractionated (primitive) and fractionated (McCOY, 1995). Silicate inclusions of the unfractionated type (Netschaevo, Techado, Watson) have chondritic compositions (McCOY, 1995), with those in Netschaevo and Techado rarely exhibiting a chondritic texture (OLSEN and JAROSEWICH, 1971; CASANOVA

et al., 1995). Silicate inclusions of the fractionated type (Weekeroo Station, Colomera, Elga, Kodaikanal) have fractionated compositions and do not have chondritic textures. Therefore, models for the origin of silicates in IIE irons should account for both the fractionated and unfractionated types.

Silicate inclusions of the fractionated type consist mainly of pyroxene and plagioclase. If the fractionated silicate inclusions were produced as crystallization products of fractionated magmas derived from the H chondritic precursor by fractional crystallization of mafic magmas, or by a low-degree of partial melting, the pyroxene in these inclusions should have lower MgO/(MgO+FeO) mole ratios (hereafter, mg ratios) than that of the precursors. However, the mg ratios of low-Ca pyroxenes in fractionated IIE silicate inclusions range from 0.85–0.76, which overlaps with those in the H chondritic precursor (mg ratios of 0.84–0.80). This discrepancy cannot be explained by an hypothesis that the IIE silicate inclusions were cumulates from fractionated magmas, because this cumulate model conflicts with the fact that the IIE silicate inclusions contain large amounts of albite, K-feldspar, silica minerals, Ca-phosphates, etc. and thus have bulk chemical compositions of fractionated silicate liquid. Any model for the origin of the fractionated IIE silicate inclusions must clarify this discrepancy, and we present our model in this report, based on new data from the silicates in the Miles meteorite.

2. Analytical Methods

Chemical compositions of the minerals were obtained with a JEOL 733 electron probe microanalyser (EPMA), using an accelerating voltage of 15 kV and probe current of 3 to 10 nA. Compositions were corrected by the BENCE and ALBEE method (BENCE and ALBEE, 1968) for silicates, oxides, and phosphates, and by the standard ZAF method for metals, sulfides, and phosphides. Bulk chemical compositions of the silicate inclusions were calculated from modal analyses in the following manner. Back-scattered-electron (BSE) images of all the silicate inclusions studied were taken, and the modal compositions of the four major components (plagioclase, low-Ca pyroxene, high-Ca pyroxene, and antiperthite-tridymite intergrowth) in each silicate inclusion were measured on the BSE images. Then, the total areal percentages of the four components were converted to weight percentages with their appropriate densities, and the bulk chemical compositions were calculated from the weight percentages of the four components by multiplying their average compositions.

3. Sample Descriptions

The Miles inclusions are 2–10 mm in size with round, ellipsoidal, and irregular shapes. Six thin sections (AMNH 4866-3, 4, 5, 6, 7, and 8) were used for this study, and each thin section comprises several silicate inclusions. In addition, one silicate inclusion in a polished section (AMNH 4866-1) has olivine and magnesian ilmenite, and this is reported together. The silicate inclusions were numbered as shown in Table 1, and the total number studied was 30.

Impact shock is clearly recorded in the Miles silicate inclusions; pyroxene and plagioclase are remarkably fractured, and most of the fractures are now filled with limo-

Table 1. Textures and mineral assemblages of the Miles silicate inclusions studied.

Inclusion	Texture	Cpx	IPig	Opx	Pl	Ant-P	Kf	Tridy	Gr-Gl	Cry-Ab	Chm	Rut	Aml	Ilm	Wht	Apt	Ol	Sod
3A	Gabbroic	++		+	++	+	+	+										
3B	"	++		++	++													
3C	"	++		++	++													
3D	"	++		++	++													
3E	"	++		++	++	+	++	+			+	+						
3F	"	++		++	++			+			+				+	+		
4A	Gabbroic	++		++	++													
4B	"	++		+	++			+										
4C	"	++		++	++													
4D	"	++	+	++	++										+			
4E	"	+		++		++	+	++		(+)								
5A	Gabbroic	++		++	++	++	+	++	+		+	+	+		+	+		
5B	"			+	++													
5C	"	+		++				+		(+)								
6A	Gabbroic	++	+	++	++				+		++	+					+	
6B	"	++		++	++												++	
6C	"	++		+		++	++	++										
6D	"	++	+	++	++	++	++	++	+								+	
6E	"	++		++	++	+		+										
7A	Cryptocry.	++				(+)	+			++								
7B	Gabbroic	++		++	++			+										
7C	"	++		++	++													
7D	"	++		++	++													
7E	"	++		++	++	+	+	+										
8A	Cryptocry.			+		(+)				++	+	+		++			+	+
8B	Gabbroic	++		++	++	+	+	+										
8C	"	++		++	++													
8D	"	++		++	++		+											
8E	"	++		++	++													
1C	Gabbroic	++		++	++		(+)				+	+		+	+		+	

++: major, +: mior, (+): trace. Abbreviations: Cpx (high-Ca pyroxene), IPig (inverted pigeonite). Opx (orthopyroxene), Pl (Plagioclase), Ant-P (antiperthite), Kf (K-feldspar), Tridy (tridymite), Gr-Gl (granitic glass), Cry-Ab (cryptocrystalline albite), Chm (chromite), Rut (rutile), Aml (armalcolite), Ilm (ilmenite), Wht (whitlockite), Apt (Cl-apatite), Ol (olivine), and Sod (sodalite).

nitic material. However, no dendritic metal-schreibersite melt pockets, like those in the Watson IIE iron (OLSEN *et al.*, 1994), were observed in the Miles host metal.

Crystallinity of the silicate inclusions is variable. Most are coarse-grained, but some are cryptocrystalline. The inclusions were classified into two types, gabbroic and cryptocrystalline (Table 1).

3.1. Gabbroic inclusions

Gabbroic inclusions are coarse-grained and show irregular or subrounded outlines (Figs. 1-1,-2). High-Ca clinopyroxene, orthopyroxene, and plagioclase are the major

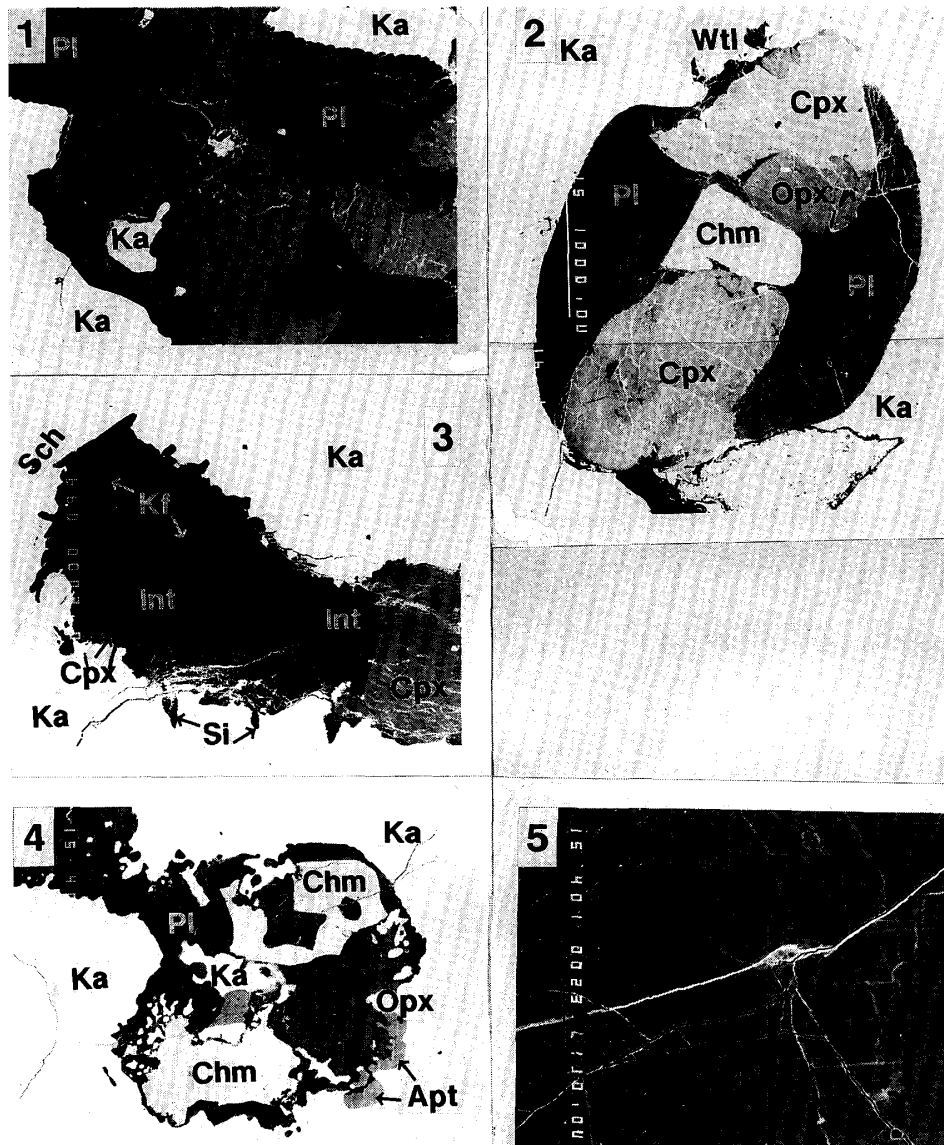


Fig. 1. Back-scattered-electron (BSE) images of Miles silicate inclusions. Abbreviation: Cpx (clinopyroxene), Opx (orthopyroxene), IPig (inverted pigeonite), Pl (plagioclase), Ant-P (antiperthite), Int (antiperthite-tridymite intergrowth), Kf (K-feldspar), Ab (albite), Crypto. Ab (cryptocrystalline albite), Si or Trid (tridymite), Gl (granitic glass), Ol (olivine), Sod (sodalite), Anor or Ant (anorthoclase), Chm (chromite), Rut (rutile), Aml (armalcolite), Ilm (ilmenite), Wtl or Whl (whitlockite), Apt (Cl-apatite), Sch (schreibersite), Tr (troilite), Ka or Met (kamacite), and Ta (taenite).

- 1-1. Coarse-grained texture of gabbroic inclusion No. 5A. Note the wavy boundary between kamacite and plagioclase (upper right). Width is about 3 mm.
- 1-2. Subrounded outline of gabbroic inclusion No. 4D. Scale bar in middle left is 1 mm.
- 1-3. Antiperthite-tridymite intergrowth of gabbroic inclusion No. 5A. K-feldspar occurs in close association with the intergrowth. Width is 1.7 mm.
- 1-4. Chromite-rich portion of gabbroic inclusion No. 6A. Width is 3 mm.
- 1-5. Exsolution lamellar texture of high-Ca pyroxene in gabbroic inclusion No. 4B. Scale bar is 100 μ m.

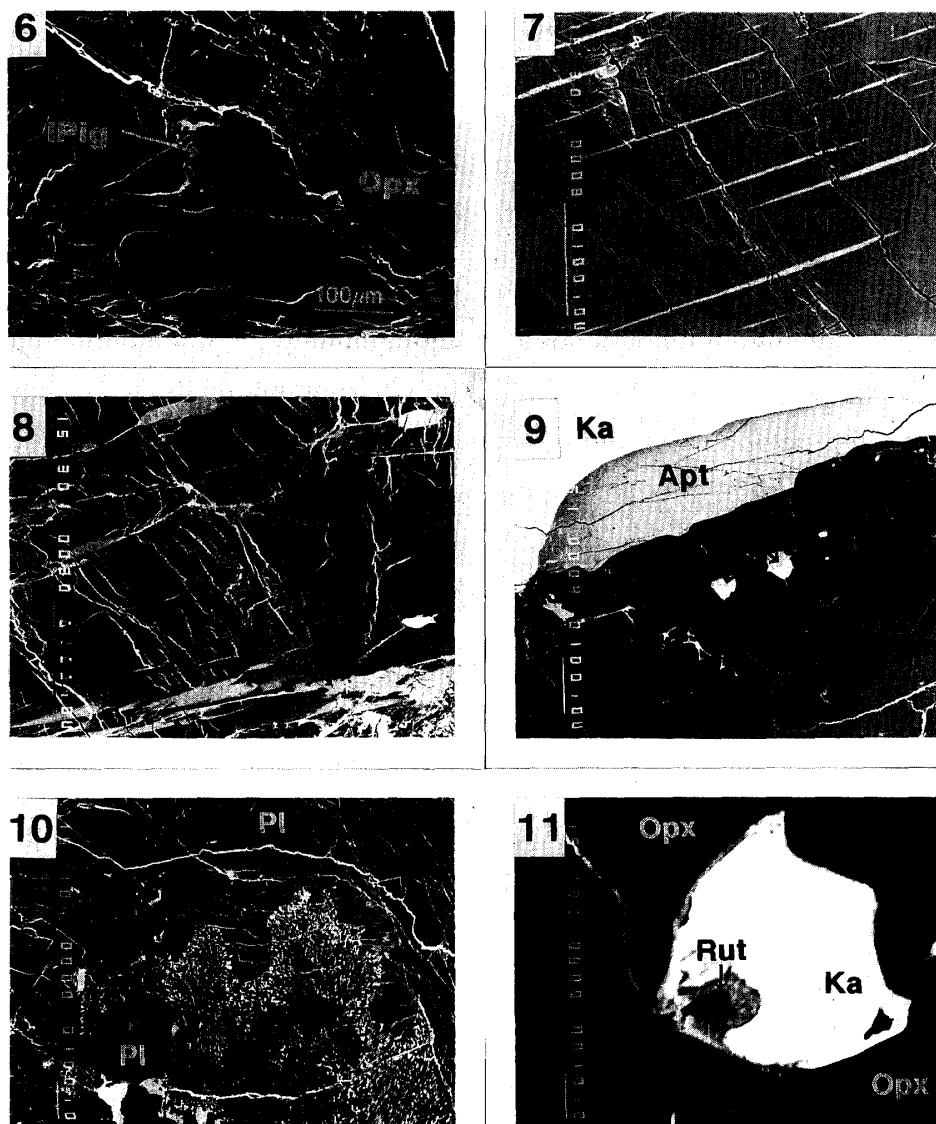


Fig. 1-6. Inverted pigeonite in large orthopyroxene, gabbroic inclusion No. 6D. Note the corroded outline of the inverted pigeonite grain. Scale bar is 100 μm .
 1-7. Exsolution lamellae of K-feldspar in plagioclase, gabbroic inclusion No. 8D. Scale bar is 100 μm .
 1-8. Antiperthite-tridymite intergrowth in gabbroic inclusion No. 4E. Scale bar is 100 μm .
 1-9. Granitic glass occurs in interstitial spaces between pyroxene grains near a large apatite grain, gabbroic inclusion No. 6A. Scale bar is 100 μm .
 1-10. Olivine occurs in close association with orthopyroxene (Opx)-whitlockite (Wht) intergrowth in gabbroic inclusion 1C. Scale bar is 100 μm .
 1-11. Magnesian ilmenite (Ilm) occurs as a small grain in contact with kamacite (Ka) in inclusion 1C, and seems to be in equilibrium with kamacite and rutile (Rut). Scale bar is 10 μm .

phases, and they are 0.5–5 mm across. Pyroxene occurs as euhedral phenocrysts, and plagioclase is anhedral; large oikocrysts of plagioclase include phenocrysts of pyroxene

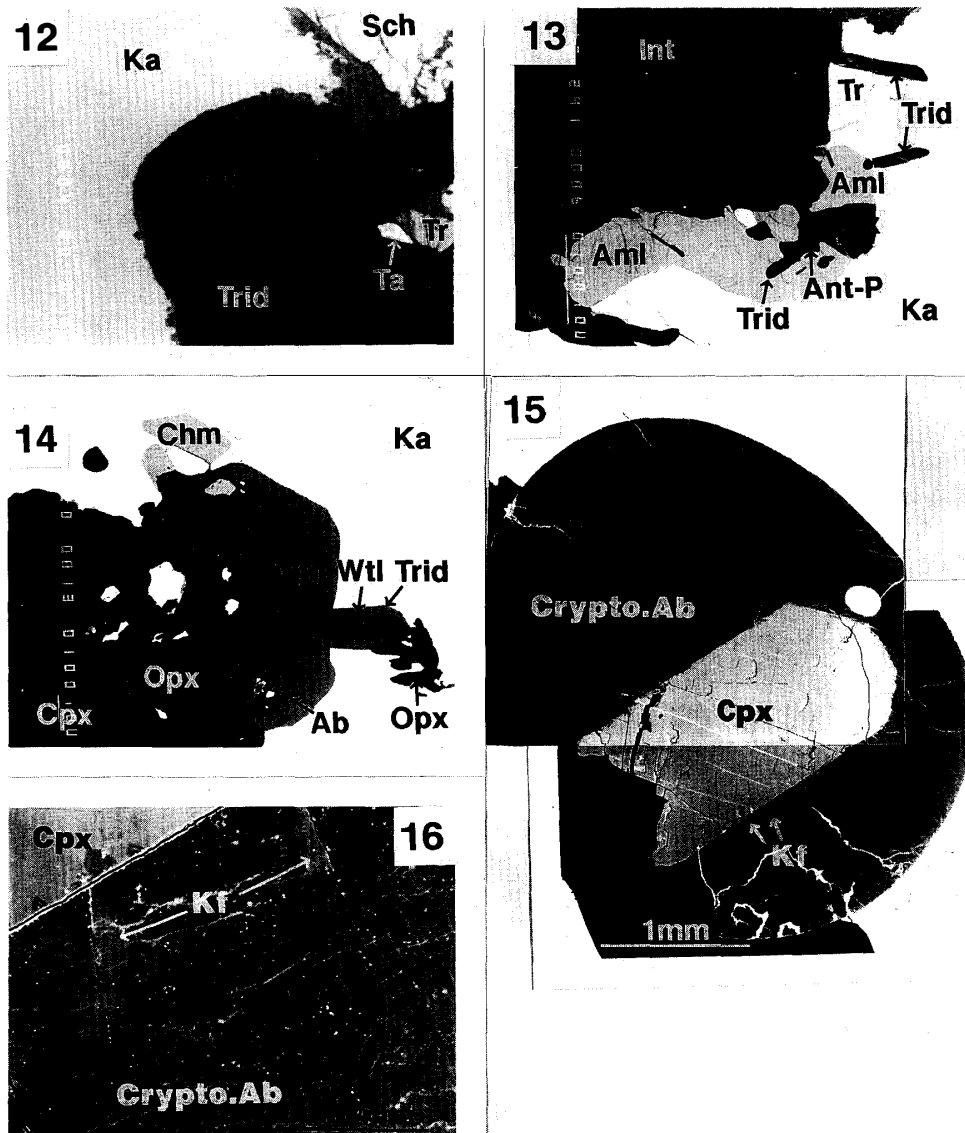


Fig. 1-12. Rutile occurs at the rim of gabbroic inclusion No. 5A. Width is 170 μm .
 1-13. Armalcolite occurs at the rim of gabbroic inclusion No. 5A. Scale bar is 100 μm .
 1-14. Cl-apatite occurs in contact with whitlockite at the rim of inclusion No. 3F. Scale bar is 100 μm .
 1-15. Cryptocrystalline inclusion No. 7A. A phenocryst of high-Ca pyroxene occurs in the central portion, and a small kamacite spherule is in the upper right. Scale bar is 1000 μm .
 1-16. Enlarged portion of inclusion No. 7A. Note the occurrence of anorthoclase streaks in close association with K-feldspar. Scale bar is 50 μm .

(Figs. 1-1,-2). Modal abundances of clinopyroxene, orthopyroxene (including inverted pigeonite) and plagioclase are highly variable, and the average composition of the gabbroic inclusions is shown in Table 2. Antiperthite-tridymite intergrowths occur in some gabbroic inclusions (Fig. 1-3) and sometimes they form complete isolated inclusions,

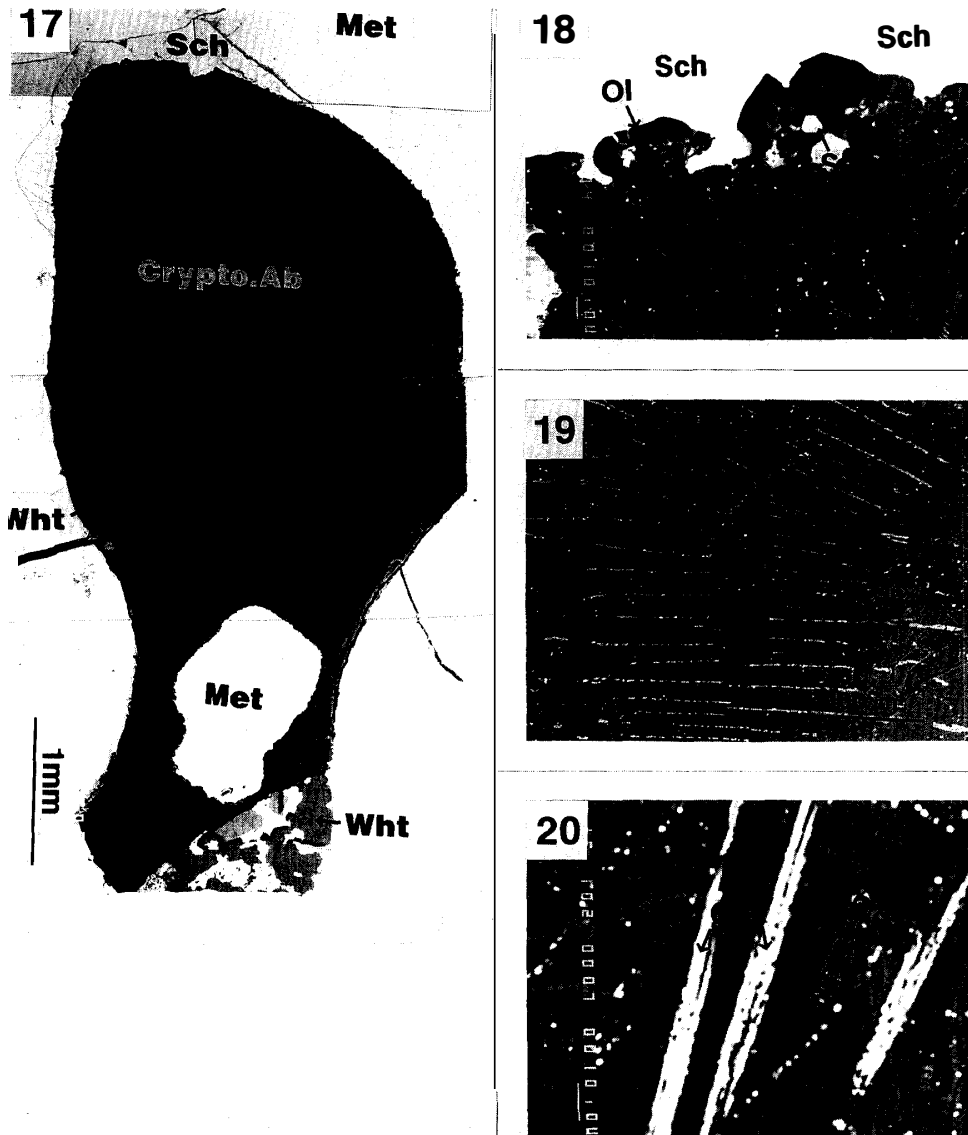


Fig. 1-17. Cryptocrystalline inclusion No. 8A. Note the occurrence of two whitlockite-predominant nodules. Schreibersite partly surrounds the inclusion (upper). Scale bar is 1000 μm .

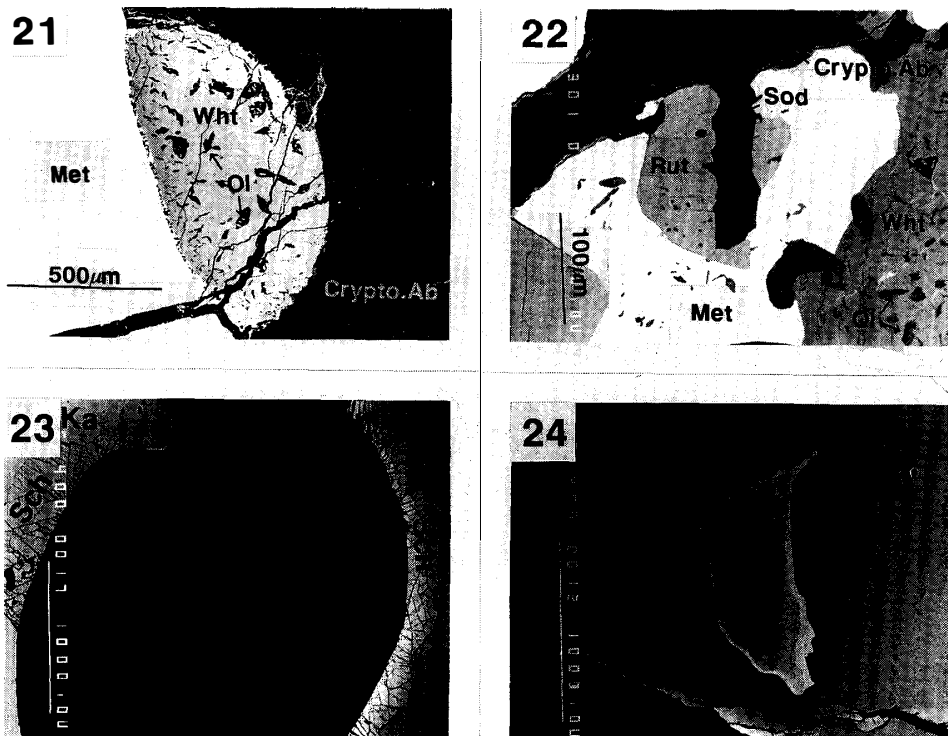
1-18. Enlarged portion of inclusion No. 8A. Olivine occurs at the boundary between schreibersite and cryptocrystalline albite. Scale bar is 10 μm .

1-19. Enlarged portion of inclusion No. 8A. Note the occurrence of needles of orthopyroxene and anorthoclase streaks in cryptocrystalline albite. Scale bar is 100 μm .

1-20. Enlarged portion of Fig. 1-19, inclusion No. 8A. Note the porous texture of cryptocrystalline albite and tiny kamacite grains (white). Scale bar is 10 μm .

which we classify as gabbroic. The intergrowths occur locally in gabbroic inclusions, and make up about 2.5 vol% on average (Table 2). In addition, a chromite-rich aggregate was found in one gabbroic inclusion (Fig. 1-4).

Large high-Ca clinopyroxene in the gabbroic inclusions commonly shows a lamellar exsolution texture (Fig. 1-5); the widths of the clinopyroxene host and orthopyroxene



- Fig. 1-21. A whitlockite-predominant nodule in inclusion No. 8A. Note the euhedral olivine grains occurring in whitlockite, and small olivine grains at the boundary between the host metal and the nodule. Scale bar is 500 μm .
- 1-22. Enlarged portion of a whitlockite-predominant nodule in inclusion No. 8A. Note that sodalite is included in rutile and partly by metal, and small euhedral olivine grains occur in the metal and whitlockite. Scale bar is 100 μm .
- 1-23. Schreibersite occurs as a mantle partly surrounding subrounded gabbroic inclusion No. 4D. Scale bar is 1000 μm .
- 1-24. Taenite included in kamacite, in the Miles host metal. Scale bar is 1000 μm .

lamellae are about 10 μm and 1 μm or less, respectively. Large orthopyroxene has no lamellar textures except when it formed as inverted pigeonite. Inverted pigeonite grains are sometimes included in large orthopyroxenes and partly by high-Ca pyroxenes, and show corroded outlines (Fig. 1-6). They consist of an orthopyroxene host and high-Ca pyroxene lamellae several micrometers wide and spaced about 25 μm apart. The areal ratio of host to lamellae is about 4:1 or 5:1.

Plagioclase is the most abundant mineral in the gabbroic inclusions. Sometimes the boundaries between the plagioclase and the host metal are wavy (Fig. 1-1). Rarely, plagioclase includes exsolution lamellae of K-feldspar (Fig. 1-7).

The accessory minerals in the gabbroic inclusions are less than 0.5 mm in size, and are antiperthite, K-feldspar, tridymite, granitic glass, olivine, chromite, rutile, armalcolite, ilmenite, whitlockite, chlorapatite, metal, and troilite. Antiperthite consists of albite and K-feldspar lamellae (Fig. 1-8) of variable width ranging from less than 1 μm to several μm . The areal ratio of albite to K feldspar is about 2:1. Antiperthite commonly occurs as an intergrowth with tridymite (Fig. 1-8); the width of antiperthite and tridymite is also variable, ranging from several to 200 μm . Small grains of tridymite, albite, or K-

Table 2. Modal compositions of the average of 27 gabbroic inclusions, and cryptocrystalline inclusion No. 8A.

Average Miles gabbroic inclusion		
High-Ca Pyroxene	33.6 vol%	(37.2 wt%)
Orthopyroxene	17.1	(19.2)
Plagioclase	46.8	(41.5)
Antiperthite-tridymite intergrowth	2.5	(2.1)
Cryptocrystalline inclusion No. 8A		
Cryptocry. albite	91.1 vol%	(90.2 wt%)
Whitlockite	6.4	(7.8)
Rutile	0.6	(1.1)
Olivine	0.6	(0.7)
Sodalite	0.3	(0.25)
Kamacite	1.1	—

Kamacite is omitted from wt% calculation.

feldspar are found at the rims of some gabbroic inclusions. K-feldspar (Fig. 1-8) occurs in close association with antiperthite-tridymite intergrowths and is up to 100 μm in width. Granitic glass is rare, its size is less than a few tens of micrometers, and it occurs in close association with phosphates; it is observed in interstitial spaces among pyroxene grains near phosphates (Fig. 1-9) or as small inclusions in phosphates. Olivine is very rare and found in one gabbroic inclusion (1C) in a polished section (AMNH 4866-1), and occurs in close association with orthopyroxene-whitlockite intergrowth (Fig. 1-10). Chromite (Fig. 1-2) is observed as euhedral grains up to 500 μm across. Magnesian ilmenite occurs in close association with kamacite and rutile in a silicate inclusion (1C) (Fig. 1-11). Rutile occurs as small grains, a few tens of micrometers across, at the rims of some gabbroic inclusions (Fig. 1-12), or in close association with chromite, sulfide, or kamacite (Fig. 1-11). Cr-Zr-Ca armalcolite occurs at the rim of a gabbroic inclusion in close association with an antiperthite-tridymite intergrowth (Fig. 1-13). It often includes small grains of antiperthite, tridymite, and pyroxene. Whitlockite and chlorapatite (Fig. 1-14) occur, often independently, rarely together, as subrounded grains at the rims of gabbroic inclusions and rarely as euhedral grains in antiperthite-tridymite intergrowths, up to a few hundred micrometers across. Troilite (or pyrrhotite, Fig. 1-13) occurs in or at the rims of gabbroic inclusions, and kamacite and taenite also occur.

The average bulk chemical composition of the 27 gabbroic inclusions studied here except inclusion 1C was calculated from the average modal composition of their four major components (high-Ca pyroxene, low-Ca pyroxene, plagioclase and antiperthite-tridymite intergrowths) (Table 2). The modal composition was multiplied by the average chemical composition of each of the components, and the results are shown in Table 3.

3.2. Cryptocrystalline inclusions

Two inclusions, Nos. 7A and 8A (Table 1), consist of cryptocrystalline materials and alkali feldspar with either a large pyroxene grain (7A) or whitlockite-predominant nodules (8A).

Cryptocrystalline inclusion No. 7A (Fig. 1-15) is ellipsoidal with a size of 2×3.5 mm, and consists of a large pyroxene lath (1×2 mm), a metal spherule (about $200 \mu\text{m}$) and cryptocrystalline material. The cryptocrystalline material is albitic in composition and is porous. It comprises irregular streaks of anorthoclase, and rare K-feldspar grains in close association with the anorthoclase streaks (Fig. 1-16).

Another cryptocrystalline inclusion No. 8A (Fig. 1-17), 3×5.5 mm, consists of two whitlockite-predominant nodules (about 1 mm across), one metal block (1.2×0.8 mm), and cryptocrystalline material. Sometimes schreibersite partly surrounds the inclusion (Fig. 1-17), and olivine grains locally occur between the schreibersite and the cryptocrystalline material (Fig. 1-18). The cryptocrystalline material consists mainly of needles of orthopyroxene, porous cryptocrystalline albite, and anorthoclase streaks (Figs. 1-19,-20). The whitlockite-predominant nodules have a curious mineral assemblage; one nodule comprises euhedral olivine grains and a few rutile grains (Fig. 1-21), and the other (Fig. 1-22) consists of sodalite, rutile, olivine, and kamacite.

The bulk chemical composition of cryptocrystalline inclusion No. 8A was calculated from its modal composition (Table 2), using the average chemical compositions of the constituent minerals, and is shown in Table 3.

3.3. Host metal

The Miles host metal is mostly kamacite, and rarely includes taenite, troilite, pentlandite, and schreibersite. Schreibersite occurs commonly as fringes which incompletely

Table 3. Chemical compositions of an average of 27 Miles gabbroic inclusions, and cryptocrystalline inclusion No. 8A, which are calculated from the modal compositions in Table 2, average H chondrite (HARAMURA *et al.*, 1983), and the calculated chemical compositions of the residues and melts for equilibrium or impact partial melting of the average H chondrite (see text). The melts for equilibrium partial melting (Equil. melting) and impact partial melting (Impact melting) are normalized to 100 wt%, and the degrees of partial melting are taken as [100 wt% minus residual total wt%].

	Averaged gabbroic inc.	Crypto. inc. No. 8A	Average H chond.	Equil. melting		Impact melting	
				Resid.	Melt.	Resid.	Melt
SiO ₂	59.46	63.86	46.60	32.18	54.58	32.16	56.12
TiO ₂	>0.18	1.58	0.13		0.49		0.51
Al ₂ O ₃	9.64	15.10	2.61		9.88		10.14
Cr ₂ O ₃	>0.90	0.01	0.60		2.27		2.33
FeO	4.65	0.63*	15.31	12.24	11.62	13.80	5.87
MnO	0.17	0.01	0.37	0.30	0.26	0.33	0.16
MgO	11.38	1.21	31.03	28.86	8.21	27.98	11.85
CaO	8.72	3.82	2.30		8.71		8.94
Na ₂ O	4.65	9.13	0.95		3.60		3.69
K ₂ O	0.25	0.88	0.10		0.38		0.39
P ₂ O ₅	—	3.78	—				
Total	100.00	100.00	100.00	73.58	100.00	74.27	100.00
mg ratio	0.81		0.78	0.81	0.56	0.78	0.78

*: about 91% of the FeO content (0.63 wt%) comes from the crypto-crystalline albite which includes magnesian orthopyroxene needles and tiny metallic Fe grains (Fig. 1-20).

surround silicate inclusions with subrounded outlines (Fig. 1-23) and less commonly surrounds silicate inclusions with irregular outlines. It occurs as irregular grains in the host kamacite. Taenite (Fig. 1-24) occurs as large grains with irregular outlines in the host kamacite, and shows a composite zonation; the core is a fine-grained plessitic intergrowth of kamacite and taenite, the mantle is massive, and the rim is Ni-rich taenite (Fig. 1-24).

4. Mineralogy

Representative chemical compositions of the constituent minerals in the silicate inclusions in Miles are shown in Tables 4 and 5.

4.1. Pyroxene

High-Ca pyroxene, $En_{45-50}Fs_{8-12}Wo_{40-45}$, is similar in composition to that in equilibrated H-group chondrites, but slightly more ferroan (Fig. 2). It has fine exsolution lamellae and the bulk composition is poorer in the Wo component (Table 4). Most of the orthopyroxene has a composition of $En_{75-78}Fs_{19-23}Wo_{1-4}$ and is slightly more ferroan than that of equilibrated H chondrites (Fig. 2), whereas orthopyroxene coexisting with olivine in inclusion 1C (Fig. 1-10) is magnesian with mg ratios of 0.88–0.84. Inverted pigeonite grains are sometimes included in large orthopyroxene grains, and the bulk composition of the inverted pigeonite was calculated, using the volume ratio of orthopyroxene host and high-Ca pyroxene lamellae and their average chemical composition, and is shown

Table 4. Representative compositions of minerals in Miles gabbroic inclusions.

	Bulk Cpx	Cpx	IPig		Bulk IPig	Opx	Ol	Pl		Anti-perth	Kf	Tridy	Gran. Glass	Chm	Rutil	Aml*	Ilm	Wht	Apt
			Host	Lamel				Olig	Ab										
SiO ₂	52.27	53.86	56.00	55.25	55.85	55.86	39.49	64.69	67.62	67.00	65.65	97.18	75.56	0.00	0.00	0.00	0.00	0.00	0.00
TiO ₂	0.49	0.25	0.00	0.21	0.04	0.16	0.00	0.13	0.13	0.14	0.05	0.31	0.23	4.68	98.23	68.63	57.50	0.00	0.00
Al ₂ O ₃	0.77	1.08	0.14	0.80	0.27	0.24	0.07	21.35	20.67	18.81	18.16	1.41	13.84	1.36	0.00	0.22	0.00	0.00	0.00
Cr ₂ O ₃	1.43	2.15	0.37	2.41	0.76	0.50	0.05	0.00	0.00	0.00	0.00	0.00	0.00	60.41	0.00	13.27	0.01	0.00	0.00
FeO	7.68	5.24	12.87	4.74	11.30	13.32	12.85	0.29	1.15	0.00	0.04	0.10	0.00	25.85	1.00	7.01	29.95	1.64	0.25
MnO	0.41	0.19	0.69	0.15	0.59	0.49	0.60	0.00	0.00	0.00	0.00	0.00	0.00	1.45	0.00	0.32	1.52	0.00	0.00
MgO	16.73	15.86	28.47	15.82	26.02	28.27	45.71	0.00	0.00	0.00	0.02	0.00	0.02	4.94	0.00	2.35	10.98	3.64	0.06
CaO	18.38	19.76	0.71	19.57	4.36	1.20	0.04	2.64	0.79	0.10	0.03	0.00	0.21	0.00	0.00	2.25	0.00	46.28	52.28
Na ₂ O	0.84	1.09	0.00	1.27	0.25	0.04	0.00	10.04	11.17	8.19	0.92	0.64	2.49	0.00	0.00	0.72	0.00	2.99	0.45
K ₂ O	0.00	0.00	0.00	0.00	0.00	0.00	0.00	0.25	0.26	5.04	15.09	0.18	6.48	0.00	0.00	0.05	0.00	0.02	0.00
ZnO														1.09		0.00			
P ₂ O ₅																0.00		45.55	41.57
Cl																			5.45
-O(Cl)																			-1.23
Total	99.00	99.47	99.26	100.22	99.44	100.09	98.82	99.39	100.80	99.29	99.96	99.82	98.82	99.87	99.23	98.44	99.85	100.12	98.82

Bulk composition (Bulk Cpx) of high-Ca pyroxene (Cpx), including orthopyroxene (Opx) lamellae, was obtained by broad beam EPMA analyses.

Bulk composition (Bulk IPig) of inverted pigeonite (IPig) was obtained from the modal composition of the host and lamellae (Lamel), multiplied by their chemical compositions.

*: The total wt% of armalcolite (Aml) contains ZrO₂ (3.07 wt%), V₂O₃ (0.35 wt%) and NiO (0.20 wt%).

Table 5. Representative compositions of minerals in Miles cryptocrystalline inclusions.

	Inclusion No. 7A			Inclusion No. 8A							
	Cpx	Crypt. Ab	Kf	Opx	Crypt. Ab	Anort	Chm	Rutil	Wht	OI	Sod
SiO ₂	54.00	68.92	65.46	54.91	71.63	69.67	0.00	0.00	0.00	38.99	36.76
TiO ₂	0.16	0.35	0.17	1.24	0.00	0.24	0.57	99.97	0.00	0.00	1.10
Al ₂ O ₃	0.94	18.71	17.89	0.08	16.84	16.84	6.21	0.00	0.00	0.00	32.03
Cr ₂ O ₃	1.62	0.00	0.00	0.00	0.00	0.00	62.79	0.11	0.00	0.05	0.00
FeO	4.69	0.19	0.16	11.17	0.29	0.04	15.09	0.00	0.81	5.42	0.09
MnO	0.28	0.00	0.00	2.03	0.00	0.00	4.50	0.02	0.08	1.05	0.00
MgO	16.72	0.00	0.00	29.01	0.05	0.02	7.88	0.02	3.50	52.18	0.00
CaO	20.87	0.61	0.38	0.51	0.01	0.14	0.00	0.00	45.66	0.01	0.00
Na ₂ O	0.50	10.88	0.96	0.12	10.66	7.24	0.00	0.00	3.00	0.01	25.03
K ₂ O	0.00	0.59	14.29	0.00	0.44	4.24	0.00	0.00	0.02	0.01	0.00
ZnO							2.30				
P ₂ O ₅									45.69	1.46	
Cl											7.33
-O(Cl)											-1.65
Total	99.79	100.24	99.32	99.06	99.91	98.43	99.34	100.10	98.87	99.16	100.68

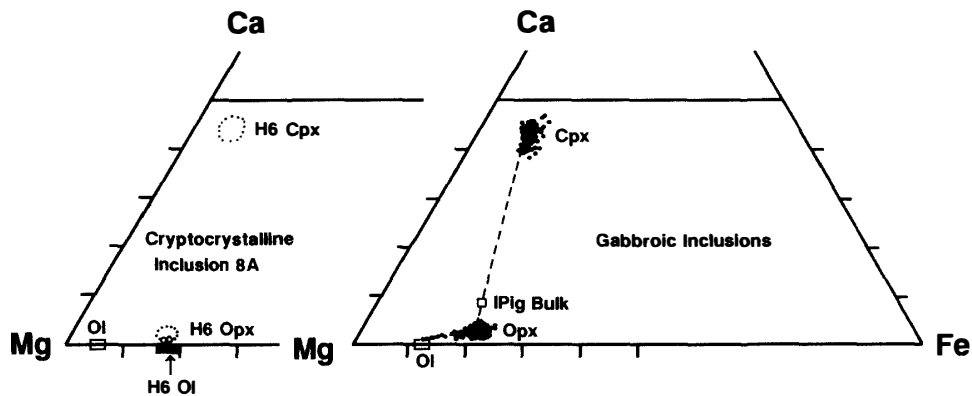


Fig. 2. Atomic Ca-Mg-Fe plot of pyroxene and olivine (Ol) in Miles gabbroic inclusions (right) and those in Miles cryptocrystalline inclusion 8A (left). Right: filled circles are high-Ca clinopyroxene (Cpx) and orthopyroxene (Opx) in the gabbroic inclusions, an open square is the bulk composition of the inverted pigeonite grains, and an open rectangle is olivine. Left: open circles and an open rectangle are orthopyroxene and olivine in cryptocrystalline inclusion No. 8A, and those in H6 chondrites are shown for reference.

in Table 4 and Fig. 2.

Some minor element contents of the pyroxenes are plotted against Al₂O₃ in Fig. 3. The Al₂O₃ contents of the pyroxenes in the gabbroic inclusions are high at the cores and decrease towards grain rims. Therefore, the arrows in Fig. 3 indicate the crystallization trends of the pyroxene; the TiO₂, Na₂O, and Cr₂O₃ contents increase from the cores to the rims for high-Ca pyroxene, but for orthopyroxene only TiO₂ increases, Na₂O is nearly constant, and Cr₂O₃ decreases from cores to rims. The MnO contents of the pyroxenes

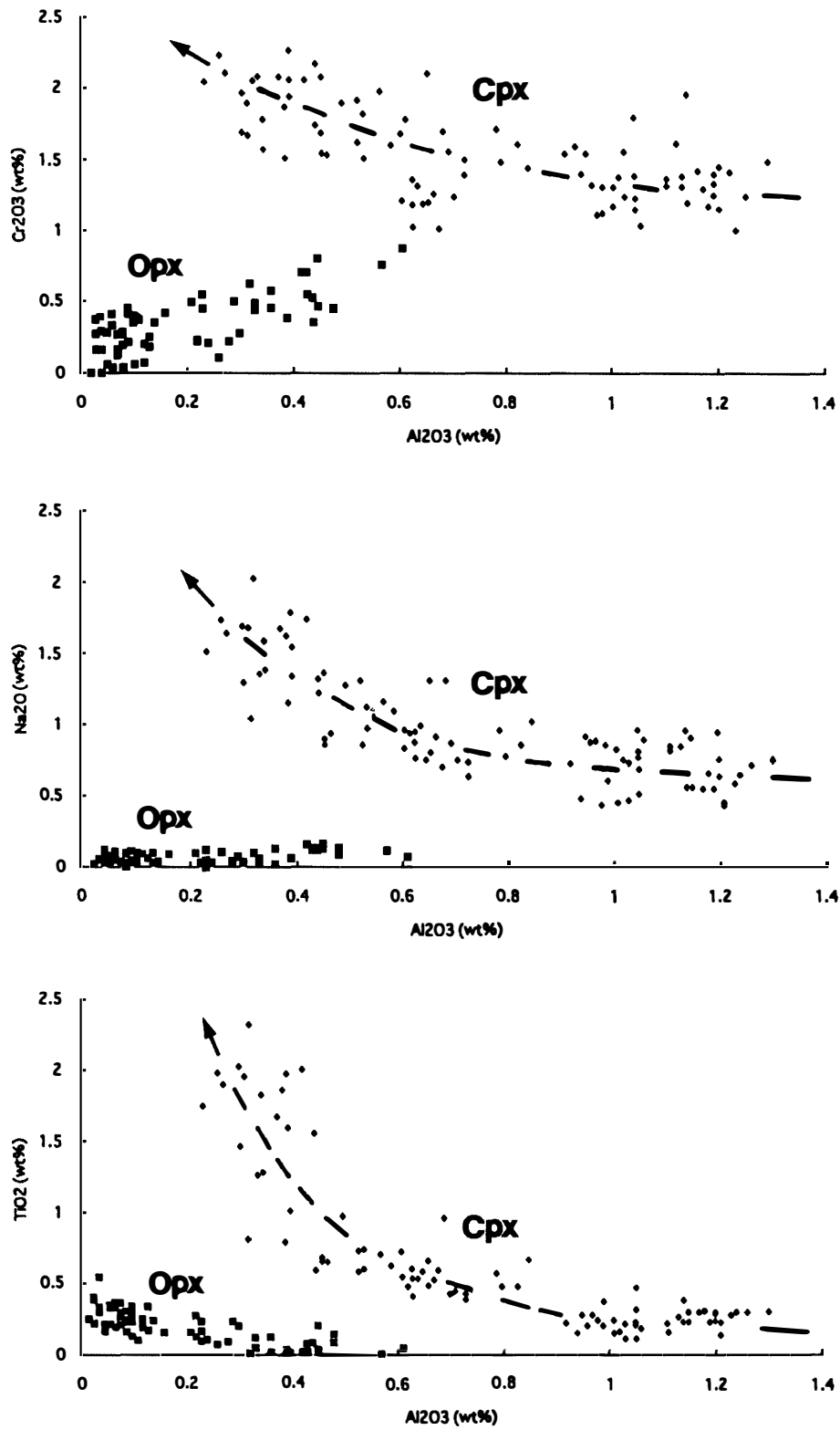


Fig. 3. TiO_2 , Na_2O , and Cr_2O_3 contents of high-Ca clinopyroxene (Cpx) and orthopyroxene (Opx) in Miles gabbroic inclusions are plotted against their Al_2O_3 contents. The arrows show the chemical trends of high-Ca pyroxene from early to late stages of crystallization.

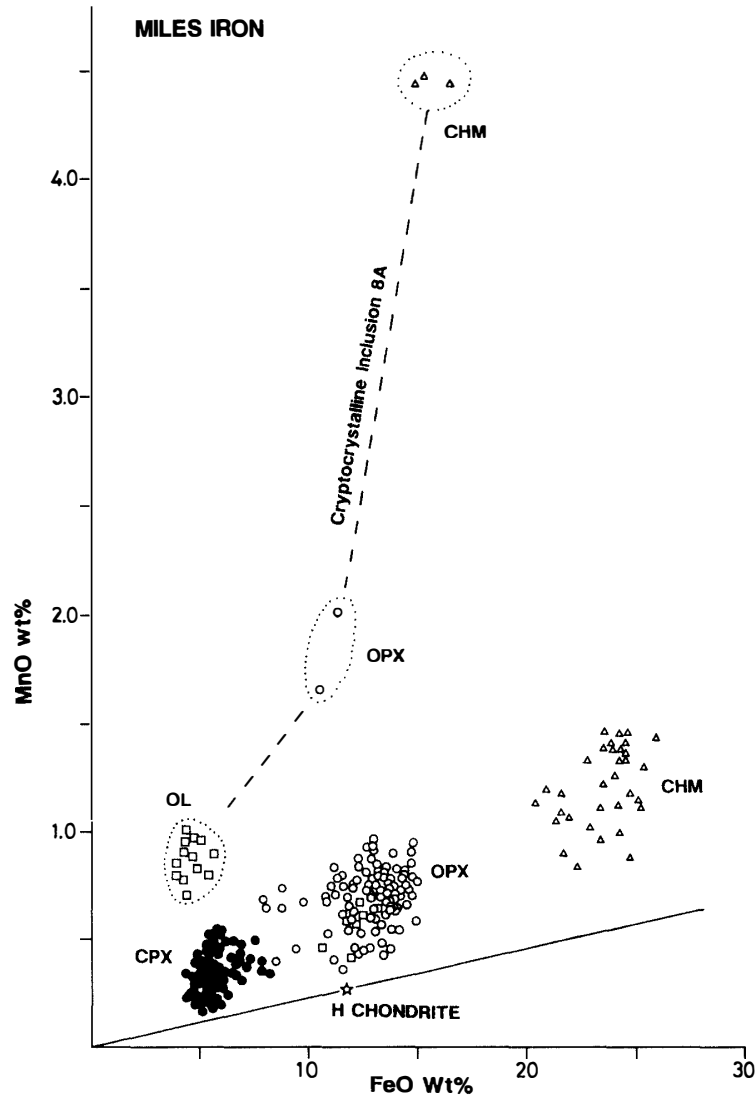


Fig. 4. MnO contents of olivine (Ol, open squares), orthopyroxene (Opx, open circles), high-Ca pyroxene (Cpx, filled circles), and chromite (Chm, open triangles) in Miles gabbroic inclusions and cryptocrystalline inclusion No. 8A. An open star is the average H chondrite. Note that the MnO contents for cryptocrystalline inclusion No. 8A are very high, although the MnO contents of high-Ca pyroxene in another cryptocrystalline inclusion, No. 7A, plot in the range of gabbroic inclusions.

are plotted against FeO in Fig. 4, indicating that their MnO/FeO ratios are higher than that of the average equilibrated H chondrites.

Orthopyroxene grains in the gabbroic inclusions show composite chemical zoning, as shown in Fig. 5. The core is moderately magnesian, the intermediate zone is ferroan, and the rim is fairly magnesian. Their minor element contents also show remarkable changes from the core to the rim (Fig. 5).

Orthopyroxene in cryptocrystalline inclusion No. 8A is present as needle-shaped

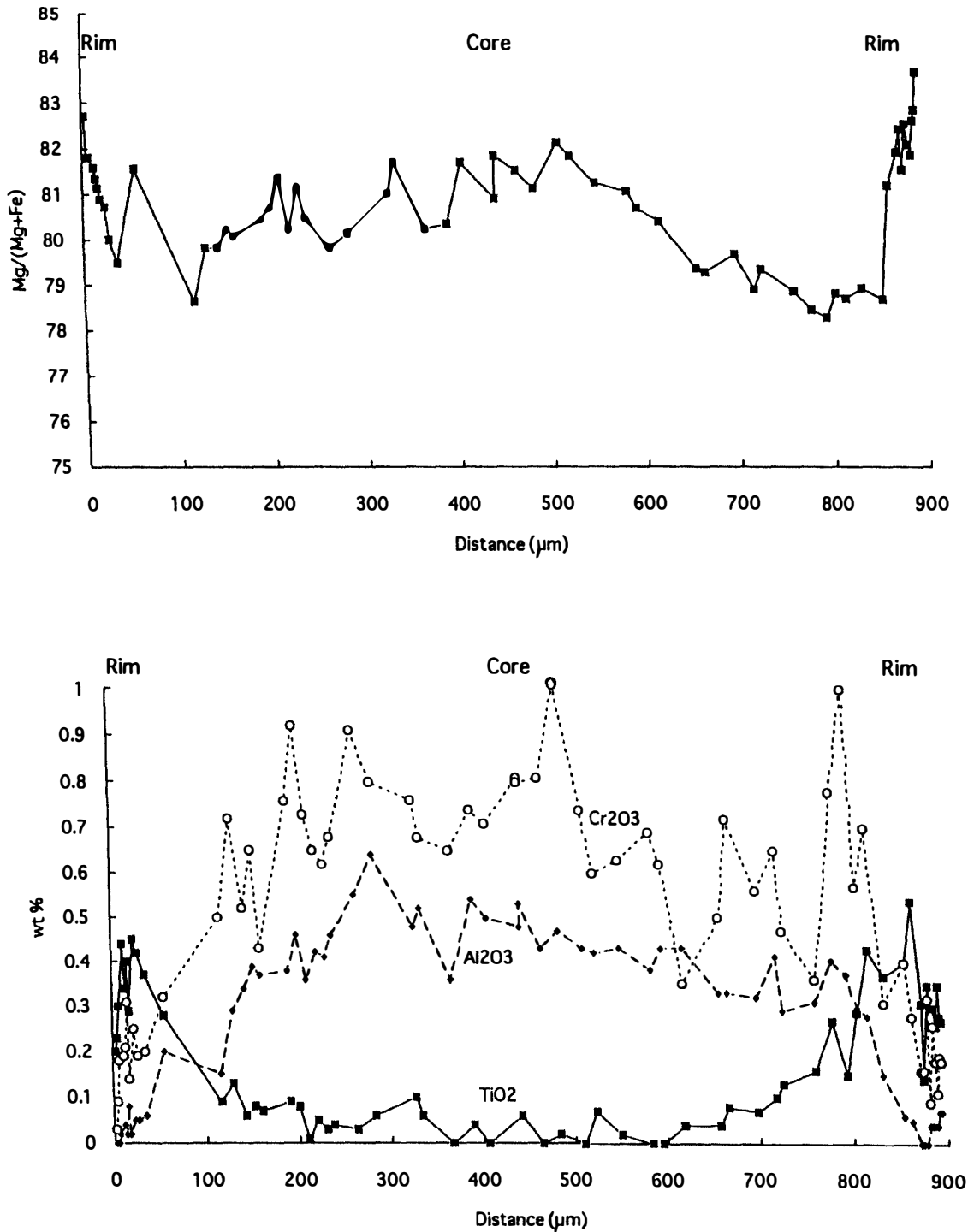


Fig. 5. Compositional zoning of an orthopyroxene grain in a Miles gabbroic inclusion, showing a cross section traversing the grain with distance in μm . Upper figure is the mg ratio (multiplied by 100), and the lower one is minor element contents in wt%.

crystals (Figs. 1-19, -20). It is enriched in MgO (Table 5), with mg ratios of 0.88–0.84 (Fig. 2) but has a low CaO content (about 1 mol% Wo). The MnO content is very high,

as shown in Fig. 4.

4.2. Plagioclase, antiperthite, and K-feldspar

Plagioclase has a wide compositional range (Fig. 6), $An_{1-15}Ab_{83-97}Or_{1-5}$, with normal zoning from calcic cores (An_{8-15}) to sodic rims (An_{2-4}). Antiperthite in antiperthite-tridymite intergrowths has a bulk composition of $An_{0-1}Ab_{60-74}Or_{25-40}$ (Fig. 6). K-feldspar

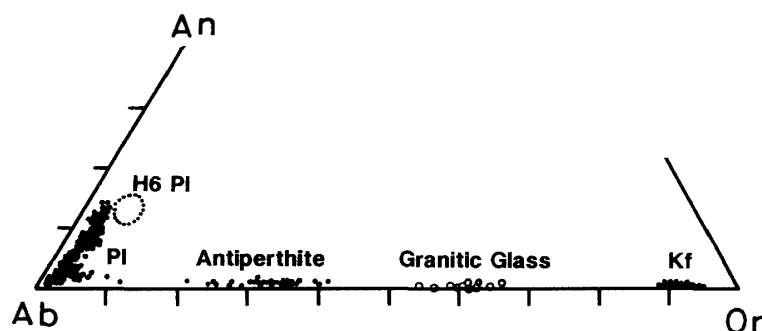


Fig. 6. Atomic plot of Ca (An, anorthite), Na (Ab, albite), and K (Or, orthoclase) of plagioclase (Pl), bulk of antiperthite, granitic glass, and K-feldspar (Kf) in Miles gabbroic inclusions. Compositional range of plagioclase in H6 chondrites is shown for reference.

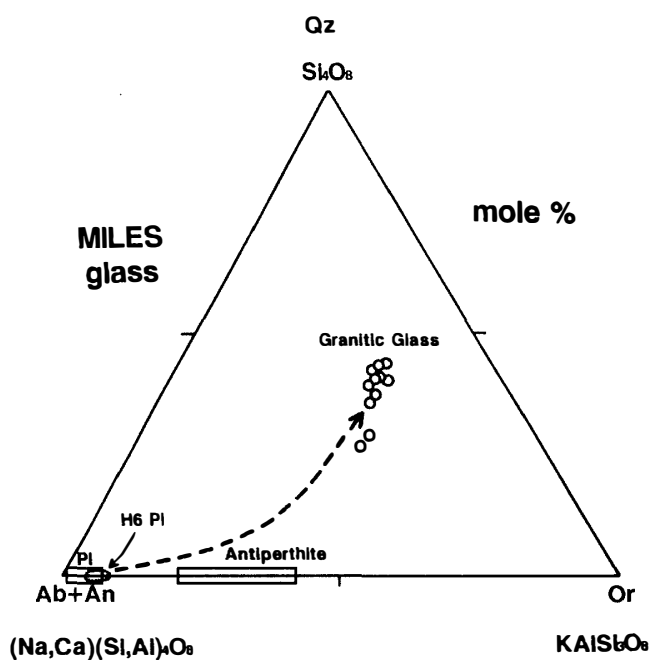


Fig. 7. Normative components of quartz (Si_4O_8), plagioclase (Ab+An), and orthoclase (Or) for granitic glass in Miles gabbroic inclusions. Compositional ranges of plagioclase and bulk antiperthite are shown by rectangles, and that of plagioclase in H6 chondrites is shown for reference. Molecular composition of quartz is taken as $O=8$, because the molecular volumes of the components are similar to each other. The arrow shows the inferred compositional trend for the residual melt to produce the granitic glass. Note that the granitic glass plots near the ternary minimum of the system Ab-Or- SiO_2 (TUTTLE and BOWEN, 1958).

grains, $\text{An}_{0.1}\text{Ab}_{5.11}\text{Or}_{88.94}$ (Fig. 6), occur in intimate association with the antiperthite (Fig. 1-8).

4.3. Granitic glass and tridymite

Granitic glass (glass having granitic compositions) occurs rarely at pyroxene grain boundaries or as small inclusions in apatite, and has a compositional range from 70–80 wt% SiO_2 , 11–15% Al_2O_3 , 6–8% K_2O , and 1.5–4% Na_2O (Figs. 6, 7). Tridymite in the gabbroic inclusions contains small amounts of Al_2O_3 and Na_2O (Table 4).

4.4. Olivine

olivine occurs in inclusion 1C (Fig. 1-10) and is $\text{Fo}_{86.89}$. It is in contact with magnesian orthopyroxene with the mg ratios of 0.88–0.84, although most of orthopyroxene in inclusion 1C is more ferroan, with the mg ratios of 0.82–0.78.

P-bearing magnesian olivine occurs at the rim of inclusion 8A (Fig. 1-18) and as small euhedral crystals in the whitlockite-predominant nodules (Figs. 1-21,-22). The magnesian olivine is $\text{Fo}_{94.96}$, more magnesian than the olivine in gabbroic inclusions. The MnO contents are high (Fig. 4), but CaO is low (Table 5), less than 0.05 wt% of the detection limit. The magnesian olivine contains variable amounts of phosphorus, ranging from 0.3–4.4 wt% of P_2O_5 (Fig. 8). The phosphorus content shows no correlation with the CaO and FeO content of the olivine, indicating that the phosphorus is not due to contamination from the surrounding Fe_3P or whitlockite. This suggests that phosphorus may replace some of the tetrahedral silicon of the olivine. Phosphoran olivine in the Zaisho pallasite, which has 4.4 wt% P_2O_5 , is in contact with P-free olivine (BUSECK and CLARK, 1984), but P-bearing olivine in Miles has different P_2O_5 contents among the grains.

4.5. Sodalite

Sodalite occurs as small grains in a whitlockite-predominant nodule in cryptocrystalline inclusion 8A (Fig. 1-22). The chemical composition is nearly stoichiometric

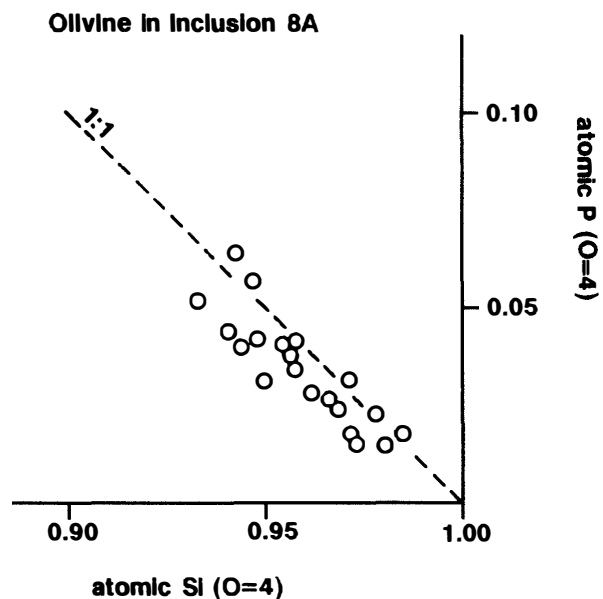


Fig. 8. Atomic P-Si plot of olivine in cryptocrystalline inclusion 8A. Phosphorus and silicon are normalized by O=4. Note that they plot along the 1:1 line.

(Table 5).

4.6. Chromite

The chemical composition of chromites within an individual gabbroic inclusion is nearly homogeneous, but is variable between gabbroic inclusions, as shown in Fig. 9. The ZnO contents of chromite in gabbroic inclusions range from 0.4 to 2.0 wt%, and show a good correlation with the Cr/(Cr+Al+2Ti) atomic ratios (Fig. 10). Chromite in cryptocrystalline inclusion 8A, which occurs at the rim between the host kamacite and the albitic cryptocrystalline material, is poor in TiO₂ (Fig. 9), and the ZnO content of the chromite is high in comparison with that of gabbroic inclusions (Fig. 10).

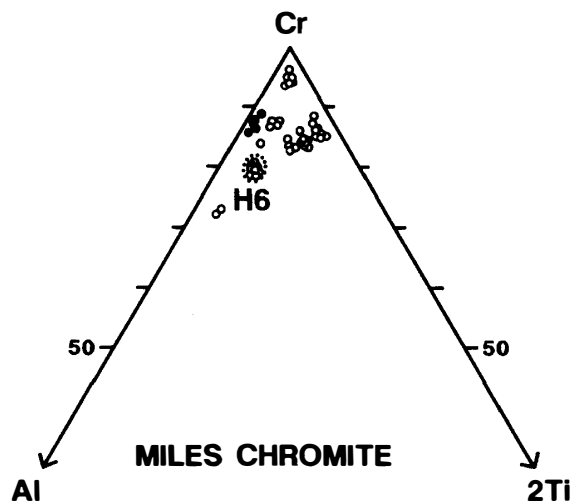


Fig. 9. Atomic Al-Cr-2Ti plot of chromites in Miles gabbroic inclusions (open circles) and cryptocrystalline inclusion 8A (filled circles). The compositional range of chromites in H6 chondrites is shown for reference. The ternary end members Al, Cr, and 2Ti represent molecular components of Al-spinel, chromite, and ulvospinel, respectively.

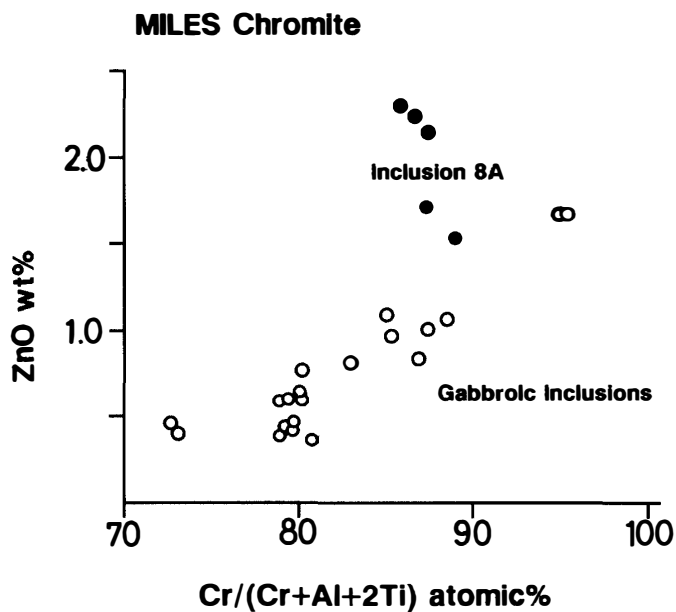


Fig. 10. ZnO contents of chromites in Miles gabbroic inclusions (open circles) and cryptocrystalline inclusion 8A (filled circles) plotted against their Cr/(Cr+Al+2Ti) atomic%. Note that ZnO of gabbroic chromites seems to increase with increasing Cr content.

4.7. Rutile, armalcolite, and ilmenite

Rutile in the gabbroic inclusions contains a small amount of FeO (Table 4), although in whitlockite-predominant nodules it is poor in FeO (Table 5). Armalcolite was found in gabbroic inclusion 5A (Fig. 1-13), and the compositional range is 67–69 wt% TiO₂, 2.9–3.3% ZrO₂, 0.2–0.3% Al₂O₃, 13–14% Cr₂O₃, 6.5–7.5% FeO, 0.3–0.6% MnO, 2.3–2.5% MgO, 2.0–2.5% CaO, and 0.5–0.8% Na₂O. This composition is similar to Cr-Zr-Ca armalcolite in lunar samples (HAGGERTY, 1973) except for high MnO, Cr₂O₃, and Na₂O and low Al₂O₃ for the Miles armalcolite. Ilmenite in inclusion 1C contains a high MgO content of about 11 wt% (Table 4), and is similar in composition to magnesian ilmenite in lunar samples which was produced by decomposition of armalcolite (HAGGERTY, 1973).

4.8. Ca-phosphate

The phosphate in the Miles gabbroic inclusions is whitlockite and chlorapatite. The chemical composition of whitlockite is similar to that in the whitlockite-predominant nodules of inclusion 8A (Tables 4, 5) except for the FeO: the content of the former is about 1.6 wt% whereas that of the latter is about 0.8%. Apatite is absent in inclusion 8A.

4.9. Sulfide, metal, and schreibersite

The sulfide in the gabbroic inclusions is troilite (or pyrrhotite). Pentlandite occurs as small grains at the rim of a troilite grain in the host metal and has 35 wt% Ni and 0.25% Co.

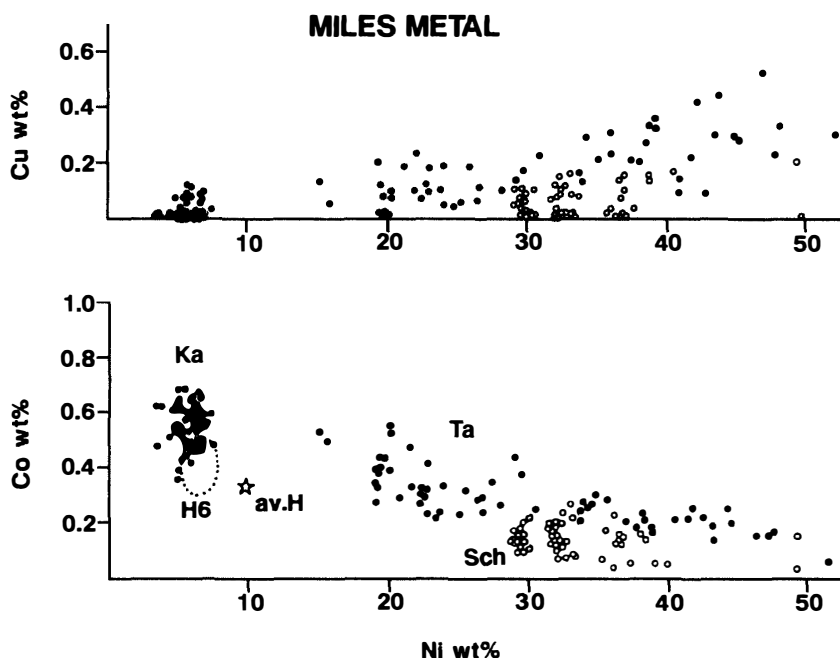


Fig. 11. Co and Cu contents of the Miles host metal and silicate-inclusion metal plotted against their Ni contents. Filled circles are kamacite (Ka) and taenite (Ta), and open circles are schreibersites (Sch). The compositional range of kamacite in H6 chondrites is shown for reference, and a star is the average metal composition of H chondrites.

Metal in the silicate inclusions is mainly kamacite and has a similar composition to the host kamacite. Kamacite is predominant in the host metal and has 3–7 wt% Ni and 0.4–0.7% Co, very similar to that in equilibrated H chondrites but slightly richer in Co (Fig. 11). Taenite is minor and has a composite compositional zoning, with Ni-poor cores and Ni-rich rims (Fig. 1-24), ranging from 15–51 wt% Ni and 0.1–0.5% Co, and the Co content decreases with increasing Ni (Fig. 11). Schreibersite also has a wide compositional range and contains 29–50 wt% Ni and minor Co (Fig. 11). Cu contents in taenites increase with increasing Ni content (Fig. 11).

5. Discussion

5.1. *Unequilibrated nature of the silicate inclusions*

Miles gabbroic inclusions have textures and mineral compositions which are similar to one another, suggesting they crystallized from a basaltic magma under similar conditions. However, the chemical compositions of the chromites differ between the gabbroic inclusions (Fig. 9), indicating that the gabbroic inclusions were not in equilibrium with each other. In addition, the coexistence of cryptocrystalline and gabbroic inclusions indicates that both types crystallized under different cooling conditions, and they have not been equilibrated. The existence of sodalite and P-bearing magnesian olivine in a cryptocrystalline inclusion and the common occurrence of tridymite in most gabbroic inclusions also indicates that the Miles inclusions were not equilibrated. Therefore, we conclude that the Miles silicate inclusions were not in equilibrium as a whole.

Techado and Netschaevo (the unfractionated type) include chondrule-like objects (OLSEN and JAROSEWICH, 1971; CASANOVA *et al.*, 1995), indicating that some silicate inclusions did not melt or recrystallize. Weekeroo Station (the fractionated type) contains two kinds of silicate inclusions, mafic and felsic (JAROSEWICH, 1990), and includes both holocrystalline and cryptocrystalline inclusions (EVENSEN *et al.*, 1979). Thus, other IIE irons with fractionated silicate inclusions are consistent with the unequilibrated nature of the Miles silicate inclusions.

5.2. *Crystallization sequence of Miles gabbroic inclusions*

Because the mineral compositions of the Miles gabbroic inclusions are very similar to those of the equilibrated H chondrites, these appear to be cogenetic. In contrast with H chondrites, most of the gabbroic inclusions are olivine-free, either the result of fractionation from an H chondritic melt, or formed by *in situ* crystallization of a feldspar-pyroxene melt produced by low-degree partial melting of an H chondritic precursor.

Textural evidence from the Miles gabbroic inclusions shows that the primary crystallizing phases were olivine and pyroxene. Magnesian olivine in inclusion 1C (Fig. 1-10) is in contact with magnesian orthopyroxene with mg ratios of 0.88–0.84, and probably crystallized prior to most of the orthopyroxene having mg ratios of 0.82–0.78. Because inverted pigeonite grains are included mainly in orthopyroxene, and partly in high-Ca pyroxene, pigeonite may have been the liquidus phase, followed by orthopyroxene and high-Ca pyroxene (Fig. 12). Inverted pigeonite grains in the orthopyroxene show corroded outlines, indicating that a reaction took place between the pigeonite and the coexisting silicate melt during the crystallization of pyroxene. Chromite is often in-

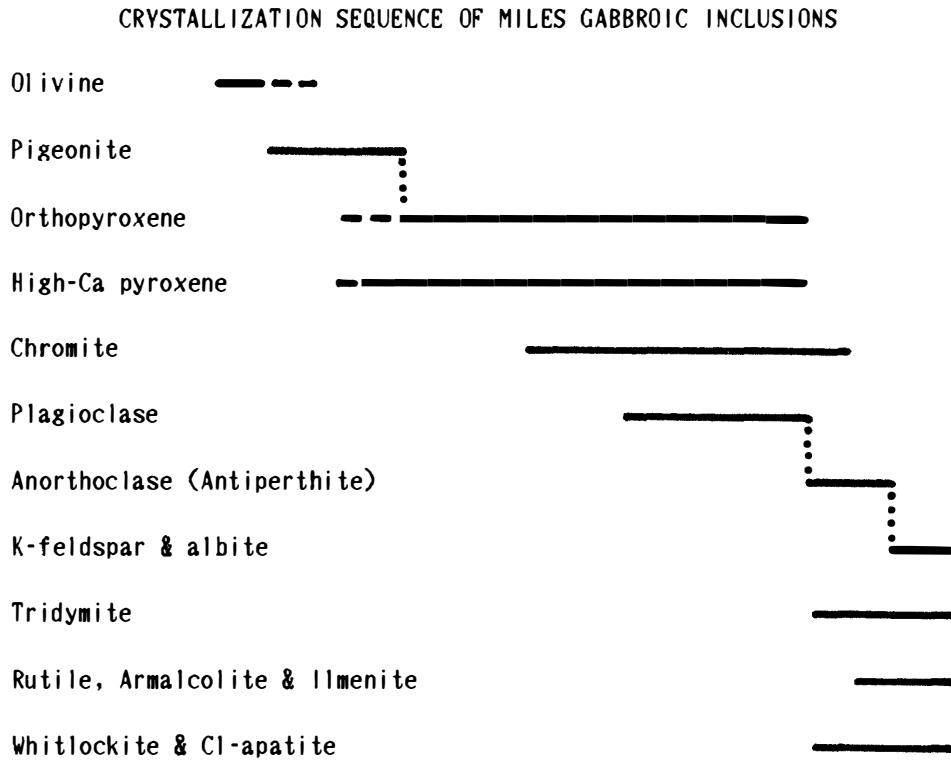


Fig. 12. Crystallization sequence of the Miles gabbroic inclusions is estimated from their textures and the occurrence of minerals. Left to right corresponds to early to late stages of crystallization.

cluded in plagioclase, and partly by pyroxene, so it may be the fifth crystallizing mineral. Plagioclase is the main phase and includes phenocrysts of pyroxene and chromite, indicating that it was the sixth crystallizing phase. Anorthoclase, which later resulted in antiperthite, crystallized together with tridymite, producing the antiperthite-tridymite intergrowths. K-feldspar and albite crystallized at the latest stage of crystallization, and probably anorthoclase decomposed to albite and K-feldspar lamellae to produce antiperthite at this latest or subsolidus stage. Negligible amounts of residual melt may have remained as granitic glass at this latest stage of crystallization. Phosphate sometimes includes a few grains of pyroxene, antiperthite, K-feldspar, albite, and tridymite, indicating that it also crystallized at the latest stage. However, chlorapatite occurs as euhedral grains in antiperthite-tridymite intergrowths, indicating that it crystallized prior to the intergrowths. Armalcolite in inclusion 5A contains antiperthite, tridymite and pyroxene, suggesting that it also formed at a late crystallization product. Rutile and ilmenite probably also formed at the latest stage. The crystallization sequence is summarized in Fig. 12.

The average bulk composition of the Miles gabbroic inclusions (Table 3) is plotted in the fundamental basalt tetrahedron of the forsterite-diopside-albite-silica system (YODER and TILLEY, 1962), and it is located near the liquidus phase boundary between forsterite and enstatite (C in Fig. 13). This is consistent with the conclusion stated above that the primary crystallizing phases were olivine and low-Ca pyroxene.

The Miles gabbroic inclusions crystallized pigeonite as a primary phase, which changed the melt composition from point C to point B in Fig. 13. Then, it was joined by

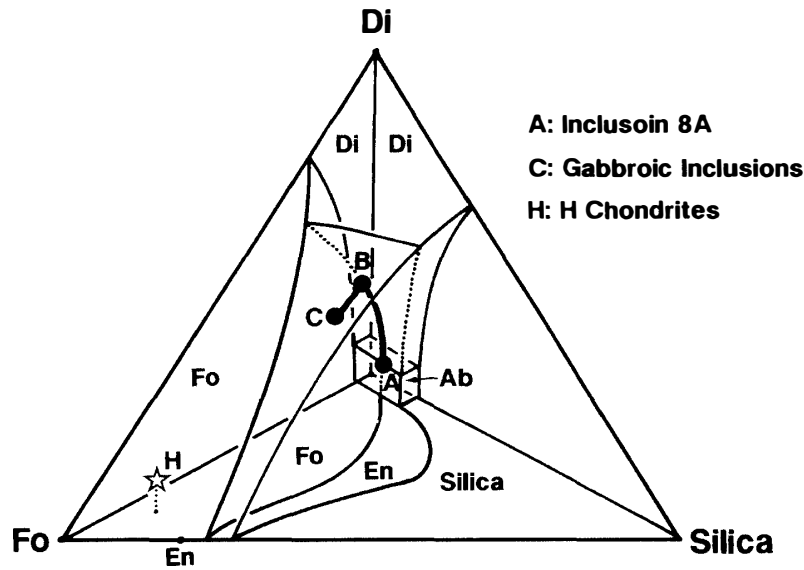


Fig. 13. Normative compositions of olivine, high-Ca pyroxene, plagioclase, and silica of cryptocrystalline inclusion No. 8A (point A), average gabbroic inclusions (point C), and average H chondrites (an open star) are plotted in the fundamental basalt tetrahedron of forsterite (Fo)-diopside (Di)-albite (Ab)-silica system (YODER and TILLEY, 1962). Point B is the crossing point of the extension line of point C and enstatite with the liquidus field boundary between the diopside and enstatite fields. The five liquidus fields are shown by Fo, En (enstatite), Di, Ab, and Silica. Note that low-degree partial melting of H chondritic precursors produces silicate melts near point A, and moderate degree (about 25%) produces basaltic melts near point C.

high-Ca pyroxene and they crystallized together with orthopyroxene, driving the residual melt toward A, where sodic plagioclase began to crystallize along with the two pyroxenes.

The Miles gabbroic inclusions may have been produced by various degrees of partial melting from H chondritic precursors. The chemical composition of the average H chondrite silicate (Table 3) is plotted in the olivine liquidus field in Fig. 13, and thus the residual minerals may be olivine at high-degrees of partial melting, or both olivine and orthopyroxene at low degrees. We calculated the chemical composition of silicate melts produced by a low degree of equilibrium partial melting from the average H chondrite using the following assumptions; (1) the amount of residual olivine is the same as that of the normative olivine in the average H chondrite, (2) the amount of residual orthopyroxene is 2/3 of the normative orthopyroxene, (3) the partition coefficient of MgO and FeO between the silicate partial melt and the residue is 0.3, (4) the Mn/Fe ratio of the residue is the same as that of the silicate partial melt, and (5) other normative components go into the silicate partial melt. With these assumptions we obtained the chemical compositions of the equilibrium silicate partial melt and the residue (Table 3). The degree of partial melting is 26.42%, and the chemical composition of the silicate partial melt is similar to that of the average gabbroic inclusion, except for the high FeO and low MgO contents of the silicate partial melt (Table 3). The mg ratio of the silicate partial melt is about 0.56 (Table 3), whereas that of the Miles gabbroic inclusions is about 0.81, which is the same as that of the residue after the equilibrium partial melting. This discrepancy in mg ratio might be explained by reduction (see later sections).

An alternative process is "instantaneous impact partial melting" of the average H

chondrite, and the assumptions for the calculations to obtain the melt composition are: (1) the amount and chemical composition of the residual olivine are the same as those of the normative olivine, (2) the amount of the residual orthopyroxene is 2/3, and the chemical composition is the same as that of the normative orthopyroxene, and (3) other normative components go into the impact partial melt. In this case, the silicate impact melt is produced “instantaneously” by impact shock and is not in equilibrium with the residue. The chemical composition of the impact melt is shown in Table 3, and is very similar to that of the average Miles gabbroic inclusion. The mg ratio of the impact melt is about 0.78, which is similar to that (0.81) of the Miles gabbroic inclusions. The degree of impact partial melting is 25.73% and is nearly the same as that of the equilibrium partial melting discussed above.

We do not know which is the main process that produced the Miles gabbroic inclusions, whether equilibrium partial melting or impact partial melting, but the Miles silicate melts may have been formed between these two extreme cases. In that case, some fraction of the FeO of the silicate melt must have been reduced.

5.3. *Crystallization of cryptocrystalline inclusions*

Cryptocrystalline inclusion 7A consists mainly of a high-Ca pyroxene phenocryst and albitic cryptocrystalline material (Fig. 1-15). Because the MnO/FeO ratio of the high-Ca pyroxene phenocryst is the same as that of the high-Ca pyroxene in the Miles gabbroic inclusions (Fig. 4), this inclusion may be cogenetic with the gabbroic inclusions. The occurrence of K-feldspar grains and anorthoclase streaks (Fig. 1-16) suggests that the cryptocrystalline material was originally antiperthite, including thin K-feldspar lamellae, and was later heated probably by impact shock, which obscured the antiperthite texture.

The bulk composition of cryptocrystalline inclusion 8A plots near point A in Fig. 13. The MnO/FeO ratios of the olivine, orthopyroxene, and chromite in the inclusion are significantly greater than those of the pyroxene and chromite in the Miles gabbroic inclusions (Fig. 4), so this inclusion might not be residual melt from the fractional crystallization of the Miles gabbroic melt (point C in Fig. 13). However, the bulk composition of cryptocrystalline inclusion 8A has a low MnO/FeO ratio (Table 3), and about 90% of the FeO comes from the tiny metal grains in the cryptocrystalline albite (Fig. 1-20). Some of the FeO in the inclusion is partitioned into the whitlockite which contains a negligible amount of MnO. Therefore, olivine in the whitlockite-predominant nodules, and orthopyroxene and chromite occurring in the cryptocrystalline albite became rich in MnO, resulting in the high MnO/FeO ratios. Therefore, this cryptocrystalline inclusion may be cogenetic with the gabbroic inclusions; it might have originally been an albite-phosphate-rich gabbroic inclusion having a similar MnO/FeO ratio, and then, impact shock might have reduced a large portion of the original FeO to the tiny metallic grains which occur in the cryptocrystalline albite.

Magnesian olivine and sodalite occur in the whitlockite-predominant nodules, showing that the nodules crystallized under silica-undersaturated conditions. On the other hand, orthopyroxene occurs in the albitic cryptocrystalline material in inclusion 8A, indicating that the cryptocrystalline material was saturated in silica component during crystallization. This discrepancy may be explained by the following hypothesis: P₂O₅-

rich melt exsolved from the albite-predominant melt by liquid immiscibility in the early stages of crystallization. This melt included a small amount of silicate component which was undersaturated in SiO_2 . P-bearing olivine and sodalite crystallized in a closed system, probably under rapid-cooling conditions. The albite-predominant melt also experienced rapid-cooling to produce the needles of orthopyroxene and the cryptocrystalline albite with porous texture (Fig. 1-20).

The cryptocrystalline material in inclusion 8A contains anorthoclase streaks (Figs. 1-19,-20) similar to that in cryptocrystalline inclusions 7A (Fig. 1-16), which might have originally been antiperthite. If so, inclusion 8A was originally an antiperthite-predominant inclusion with a large amount of phosphate, which experienced impact shock to produce a melt. The melt then separated into two melts, one albite-predominant and the other P_2O_5 -predominant, by liquid immiscibility.

5.4. *Temperatures of crystallization and cooling conditions*

The phase diagram of the fundamental basalt tetrahedron (Fig. 13) suggests that the average chemical composition of the Miles gabbroic inclusions (point C) wholly melts at a temperature of about 1300°C . Using the bulk composition of the inverted pigeonite (Table 4), the two pyroxene geothermometer (LINDSLEY and ANDERSEN, 1983) gives a temperature of about 1200°C for crystallization of the pigeonite. The pigeonite geothermometer (ISHII, 1975) gives about 1180°C for the pigeonite. The two pyroxene geothermometer gives $1150\text{--}1200^\circ\text{C}$ for the lamellar high-Ca pyroxene of the inverted pigeonite, indicating that the pigeonite inverted to the orthopyroxene host and high-Ca pyroxene lamellae just after the crystallization of the pigeonite. Using the bulk composition of the large high-Ca pyroxene cores (Table 4) which include orthopyroxene lamellae, the two pyroxene geothermometer gives about 1150°C . Rims of high-Ca pyroxene, free from orthopyroxene lamellae, or small high-Ca pyroxenes occurring in close association with antiperthite-tridymite intergrowths, give about 1100°C for their crystallization temperature. The orthopyroxene-chromite geothermometer (MUKHERJEE *et al.*, 1990) gives about 1000°C for orthopyroxene and chromite assemblages in the Miles gabbroic inclusions.

The albite-K-feldspar-silica system (SCHAIRER, 1950) indicates that both anorthoclase and tridymite crystallize in the temperature range of 1062°C to 990°C , which may be near the subsolidus temperature of the Miles gabbroic inclusions. Anorthoclase decomposes to albite and K-feldspar at temperatures around 700°C to produce antiperthite (MUELLER and SAXENA, 1977), and the feldspar geothermometer (STORMER and WHITNEY, 1977) for the coexistence of sodic plagioclase ($\text{An}_1\text{Ab}_{95}$) and K-feldspar ($\text{An}_{0.5}\text{Or}_{90}$) gives about 400°C for the equilibrium temperature. The schreibersite-kamacite equilibrium (ROMIG and GOLDSTEIN, 1980) indicates that P-bearing kamacite exsolves at temperatures of $400\text{--}500^\circ\text{C}$, and the binary system of Fe and Ni (REUTER *et al.*, 1989) suggests that taenite rims surrounding taenite grains in the Miles host metal coexist with kamacite at temperatures of $300\text{--}400^\circ\text{C}$.

The coarse-grained textures of the Miles gabbroic inclusions indicate that they crystallized under slow-cooling conditions. The existence of inverted pigeonite, and high-Ca pyroxene having exsolution lamellae, means that they cooled slowly. Using the Ca-Mg diffusion coefficient (BRADY and McCALLISTER, 1983), the homogenization time for

pyroxene, including exsolution lamellae, can be expressed by the equation, $2Dt > L^2$ where D , t , and L are diffusion coefficient, time, and distance between host and lamellae, respectively. The application of this equation to Miles inverted pigeonite, with a distance of about 15 μm , gives an homogenization time of about 160 years at a temperature of 1150°C, and about 58 years at 1200°C. High-Ca pyroxene with orthopyroxene lamellae, with a distance of about 6 μm , gives an homogenization time of about 80 years at a temperature of 1100°C, and about 26 years at 1150°C. The homogenization times obtained suggest that the Miles gabbroic inclusions cooled slowly at a high temperature range. However, the Miles gabbroic inclusions rarely contain granitic glass, indicating that they cooled rapidly at the latest stage of crystallization. The width of the antiperthite is very thin, ranging from less than one to several micrometers. The equation given above, and the inter-diffusion coefficient of K and Na in alkali feldspar with a composition of Or_{40} (CHRISTOFFERSEN *et al.*, 1983), give an homogenization time of about 10 days at a temperature of 700°C for antiperthite, with a distance of one micrometer. This rapid cooling seems to be consistent with the existence of granitic glass in the Miles gabbroic inclusions. In addition, the existence of fine-grained plessite in taenite grains in the Miles host metal suggests that the Miles iron cooled rapidly in the low temperature range. Therefore, the cooling rate is slow in the high temperature range, and rapid in the low temperature range.

On the other hand, the cryptocrystalline inclusions suggest that they cooled very rapidly. Probably they were originally albite-rich gabbroic inclusions which later experienced impact shock and wholly melted by local stress concentrations in the Miles iron. However, most of the gabbroic inclusions did not melt, but experienced intense fracturing.

5.5. Reduction

The Miles gabbroic inclusions appear to have experienced reduction during their crystallization. The lines of evidence for the existence of reduction are as follows: (i) Pigeonite crystallized prior to orthopyroxene in the Miles gabbroic inclusions, whereas orthopyroxene crystallizes prior to pigeonite in terrestrial basalts, as shown in Fig. 14. (ii) Large orthopyroxene grains in Miles show reverse zoning on their rims (Fig. 5). (iii) If the gabbroic inclusions were produced from H chondritic precursors, the Mn/FeO ratios of the minerals in the gabbroic inclusions would be the same as those in the equilibrated H chondrites. However, they are higher, as shown in Fig. 4. (iv) Equilibrium partial melting of H chondrite precursors would produce ferroan melts which have mg ratios lower than those (0.84–0.80) of equilibrated H chondrites (Table 3, Fig. 14). The Miles gabbroic inclusions have mg ratios overlapping with those of the equilibrated H chondrites (Fig. 2). As discussed above, the melts for the Miles gabbroic inclusions may have been produced by processes which are intermediate between equilibrium and impact partial melting. If so, some portion of the FeO would be reduced. (v) Schreibersite is a common mineral in Miles, although it does not occur in equilibrated H chondrites. (vi) Rutile and metallic iron often occur in contact with one another (Fig. 1-12), and magnesian ilmenite rarely occurs in Miles. Mg-free ilmenite is sometimes found in equilibrated H chondrites, and this means that Miles crystallized under lower oxygen fugacity conditions than did the equilibrated H chondrites.

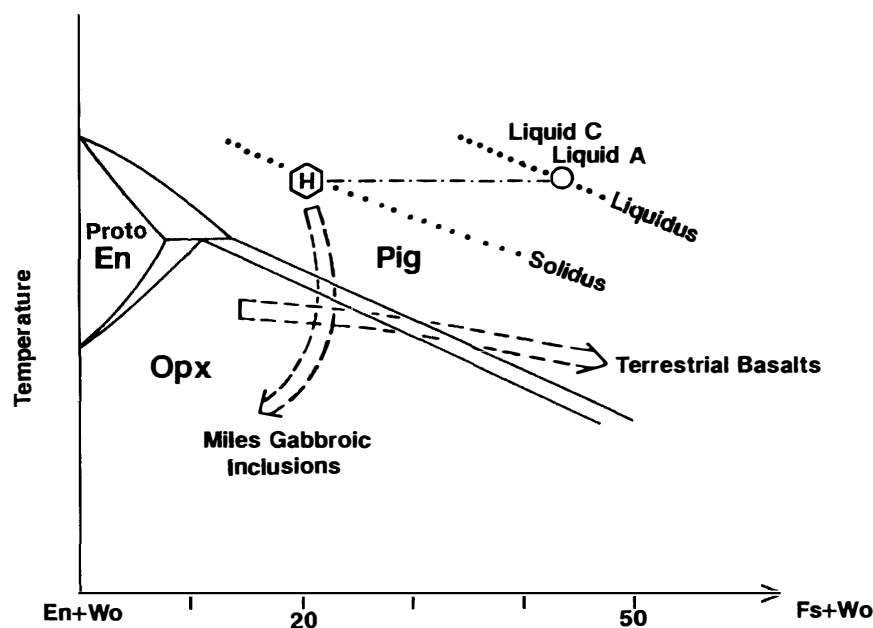


Fig. 14. Crystallization sequence of low-Ca pyroxene in Miles gabbroic inclusions is shown in the pseudobinary phase diagram of the enstatite (En)-ferrosilite (Fs) system. Stability fields of protoenstatite (Proto En), pigeonite (Pig), and orthopyroxene (Opx) are shown. The crystallization trend of low-Ca pyroxene in terrestrial basalts is shown for reference. Schematic liquidus and solidus for the Miles gabbroic inclusions are shown by dotted lines (see text).

The oxygen fugacity for the equation, $\text{FeSiO}_3 = \text{Fe} + \text{SiO}_2 + 1/2\text{O}_2$, is shown by the hatched zone in Fig. 15, for Miles orthopyroxene with a composition of Fs_{20} . The activity of iron was taken as 1 because metallic iron may have always coexisted with pyroxene. The SiO_2 on the right side of the equation is a silica component of the magma which crystallized the Miles orthopyroxene. The activity of ferrosilite was taken as 0.2, and the formational Gibbs free energy of FeSiO_3 was calculated from the thermodynamic data of WILLIAMS (1971) and ROBIE *et al.* (1979); the hatched zone in Fig. 15 is bounded by two lines, one for a silica activity of 1 (lower boundary of the hatched zone), and the other for a silica activity of 0.1 (upper boundary of the hatched zone).

The reaction line for the ilmenite-rutile-iron equation, $\text{FeTiO}_3 = \text{TiO}_2 + \text{Fe} + 1/2\text{O}_2$, is also shown in Fig. 15. Magnesian ilmenite in Miles has a mg ratio of about 0.4 (Table 4) and seems to be in equilibrium with kamacite and rutile (Fig. 1-11). On the assumption that ilmenite is an ideal solution, the magnesian ilmenite-rutile-iron equation gives oxygen fugacities of $10^{-23.5}$ at 1000 K and $10^{-13.4}$ at 1500 K, which are slightly lower than those of the Mg-free ilmenite-rutile-iron equation and near the lower boundary of the hatched zone in Fig. 15. Since rutile coexists with metallic iron in most of the gabbroic inclusions, the oxygen fugacity for the silicate inclusions may be represented by the narrow zone between the reaction line for the Mg-free ilmenite-rutile-iron equation and the line for the silica activity of 1 (lower boundary of the hatched zone). Therefore, the oxygen fugacity for the Miles gabbroic inclusions is around $10^{-13.0}$ to $10^{-13.5}$ bars at a temperature of 1500 K, and around $10^{-16.0}$ to $10^{-16.5}$ bars at a temperature of 1300 K.

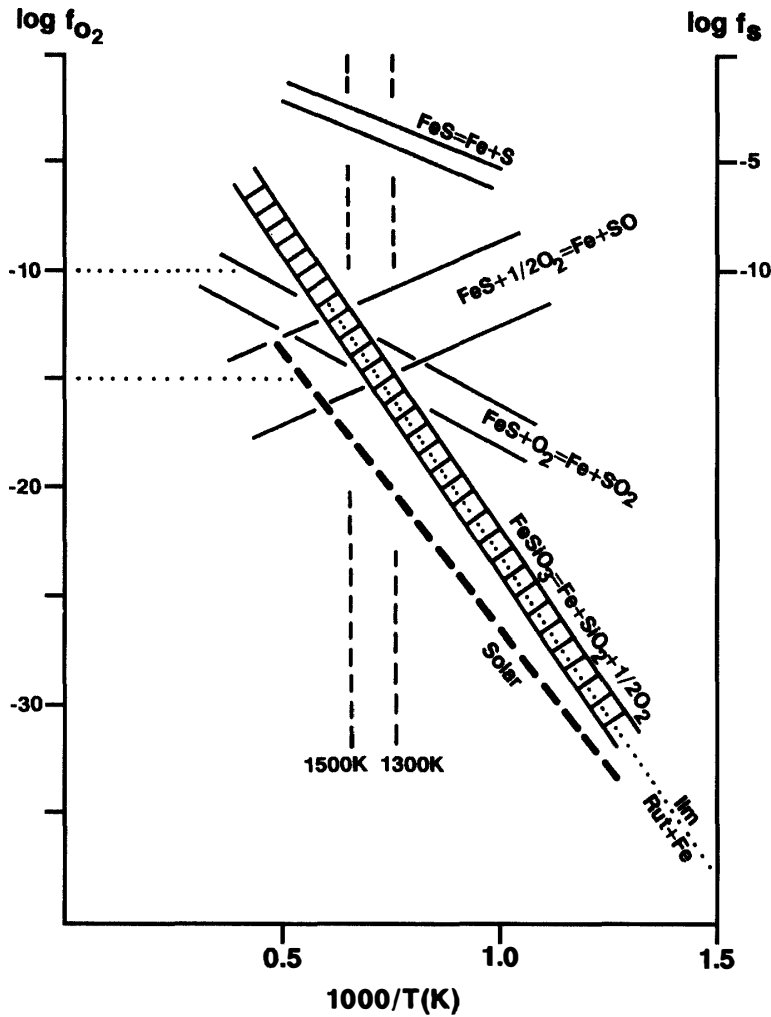


Fig. 15. Oxygen fugacities (in bars) are shown for the reactions, $FeSiO_3=Fe+SiO_2+1/2O_2$ (hatched zone, where the activity of ferrosilite is taken as 0.2; the upper boundary is defined for silica activity to be 0.1; the lower boundary is for silica activity to be 1), $FeTiO_3=Fe+TiO_2+1/2O_2$ (dotted line; Ilm: ilmenite; Rut: rutile), $FeS+O_2=Fe+SO_2$ (white zone; the upper boundary is defined for SO_2 fugacity of 10^{-6} bars and FeS activity of 1, or for SO_2 fugacity of 10^{-7} bars and FeS activity of 0.1; the lower boundary is for SO_2 fugacity of 10^{-8} bars and FeS activity of 1, or for SO_2 fugacity of 10^{-9} bars and FeS activity of 0.1), and $FeS+1/2O_2=Fe+SO$ (white zone; the conditions are the same as those for the equation $FeS+O_2=Fe+SO_2$). The line for a SO/SO_2 fugacity ratio of unity is located near the reaction line for the equation of ilmenite-rutile-iron. Oxygen fugacity of the solar gas (GROSSMAN, 1972), with a total gas pressure of 10^{-4} bars, is shown by a dashed line for reference. Sulfur fugacity is also shown for the reaction, $FeS=Fe+S$ (white zone; the upper boundary is defined for activity ratio of Fe and FeS to be 1; the lower boundary is for activity ratio of Fe and FeS to be 10).

If the gabbroic inclusions were produced by partial melting of H chondritic precursors, both silicate melt and Fe-S melt were probably produced. However, sulfide in the Miles iron occurs only in negligible amounts, and thus a large amount of the sulfur originally in the Fe-S melt was lost. The reaction for the loss of sulfur may be written by

the following equations:



where FeS is an FeS component of the Fe-S melt or troilite, and Fe is an Fe component of the Fe-S melt or metallic iron. The oxygen fugacities of eqs. (1) and (2) were calculated using thermodynamic data (JANAF and ROBIE *et al.*, 1979), and the results are shown in Fig. 15 for two cases with constant SO or SO₂ fugacities of 10⁻⁶ bars (upper line of the paired parallel lines) and 10⁻⁸ bars (lower line) on the assumption that the FeS activity is 1. For the case with the FeS activity of 0.1, the paired parallel lines correspond to constant SO or SO₂ fugacities of 10⁻⁷ bars (upper line) and 10⁻⁹ bars (lower line), respectively. Therefore, the fugacities of both SO and SO₂ for the Miles gabbroic inclusions are equal to, or lower than, 10⁻⁶ bars at a temperature of 1500 K and 10⁻⁸ bars at a temperature of 1300 K.

The fugacity of S obtained from eq. (3) is also shown in Fig. 15; it is 10^{-2.5} bars for an activity ratio of Fe/FeS of 1, to 10^{-3.5} bars for the activity ratio of 10 at a temperature of 1500 K, and 10^{-3.5} to 10^{-4.5} bars at a temperature of 1300 K. If a gas coexisted with the Fe-S and silicate melts which were produced by equilibrium or impact partial melting, the major gas components may have been SO, SO₂, S, S₂, and O₂, and among them the main species of the gas is S. Therefore, the total gas pressure for Miles Fe-S and silicate melts might be less than 10⁻² bars at a temperature of 1500 K, and 10⁻³ bars at a temperature of 1300 K.

Total pressures of a parent body with a homogeneous density of chondrites (3.4 g/cm³) are expressed by the equation, $P(\text{bars}) = 1.6 \times 10^{-2} d(D-d)$, where d and D are depth (km) from the surface and diameter (km) of the parent body, respectively. If an H chondrite parent body has a diameter of 100 km, depths of 100 m and 10 m correspond to 0.16 bars and 0.016 bars, respectively. Therefore, the low total gas pressures estimated above at the temperature range of 1500–1300 K suggest that the gas phase may not have coexisted with the Fe-S and silicate melts at levels deeper than 10 m in the parent body with a diameter larger than 50 km.

Most of the S may have dissolved in the metallic melt, and this sulfur must have escaped into space by vaporization from the surface of the mixture of the Fe-FeS and silicate melts. These melts may have been located near the surface of their parent body, suggesting that they were produced in surficial regolithic breccias on an H chondrite parent body. Metallic iron dissolves a small amount of oxygen (RINGWOOD, 1979), and this oxygen may also have escaped into space if the system is in a surficial region of the parent body. If so, oxygen may have continued to escape from the Fe-S and silicate melt mixture system, and some amount of FeO and P₂O₅ in the silicate melt may have been reduced to Fe and P which went into the Fe-S melt. The reduction of the FeO component in the silicate partial melt may have been caused by such a process, and some amount of oxygen and most of the sulfur may have been lost from the Fe-S melt during the early stages of crystallization. The reduction processes discussed above may explain the common occurrence of schreibersite and the rare occurrence of sulfide in the Miles iron. In

addition, crystallization of pigeonite prior to orthopyroxene may also be explained by such a reduction process.

The ratio of SO_2 fugacity to S fugacity is less than 10^{-4} , indicating that SO_2 and SO are minor species and the sulfur content of the Fe-S melt can reduce a small amount of FeO of the silicate melt. An additional reducing agent may be phosphorus in the Fe-S melt, and the equation, $2\text{P} + 5/2\text{O}_2 \rightarrow \text{P}_2\text{O}_5$, means that metallic P in the Fe-S melt reduces some fraction of the FeO of the silicate melt to produce the phosphate component in the silicate melt during crystallization. In the later stages of crystallization, phosphorus in the Fe-S melt can reduce a small amount of FeO in the silicate melt by this process. This may explain the reverse zoning of the Miles orthopyroxene.

5.6. Scenario

An H chondrite parent body was probably covered by a thick regolithic breccia, which was a porous aggregate. Impact shock on the surface resulted in high temperatures, up to more than 1200°C , causing equilibrium or impact partial melting of the regolithic breccia. Partial melting produced silicate and Fe-S melts, and the degrees of partial melting of the Miles gabbroic inclusions varied, but was about 25% on the whole for the silicate system. The melts separated, leaving the residues behind. The silicate melts were mixed as small inclusions in the Fe-S melt. Reduction took place as the result of oxygen escape from the silicate melts into space via the Fe-S melt, and sulfur also escaped from the Fe-S melt into space. By these processes, some amount of FeO and P_2O_5 in the silicate melt was reduced to Fe and P, which diffuses into the Fe-S melt. During reduction, crystallization of the silicate melt took place, with olivine and pigeonite crystallizing first, followed by orthopyroxene, high-Ca pyroxene, and sodic plagioclase, forming the gabbroic texture. In the latest stages of crystallization, anorthoclase and tridymite crystallized to form antiperthite-tridymite intergrowths. At the same time, rutile, magnesian ilmenite, armalcolite, K-feldspar, albite, whitlockite, chlorapatite, and sulfides precipitated in the gabbroic inclusions. The cooling rate was slow in the high temperature range and rapid in the low temperature range of crystallization.

After the cooling of the gabbroic inclusions, impact shock caused melting of some silicate inclusions by local stress concentrations, although most of the silicate inclusions remained unmelted; some experienced intense fracturing. Some albite-rich inclusions were melted by the impact shock, resulting in cryptocrystalline inclusions which cooled under very rapid cooling conditions. An albite- and phosphate-rich melt (cryptocrystalline inclusion 8A), was produced by such an impact shock, separated by liquid immiscibility into two liquids, an albite-rich silicate melt and a silica-undersaturated phosphate melt. MnO-rich needles of orthopyroxene and cryptocrystalline albite were produced from the albite-rich melt by quenching, and the whitlockite-predominant nodules formed from the silica-undersaturated phosphate melt; MnO-rich P-bearing magnesian olivine and sodalite crystallized in the phosphate melt.

Acknowledgments

We thank Dr. R. HUTCHISON for revision of our manuscript. This study was partially supported by funds from NASA grant NAGW 34-90 (to M. P.), and partially by funds for

Japan-Korea Joint Research on Antarctic Meteorites (to Y. I.), which are greatly appreciated.

References

- BENCE, A.E. and ALBEE, A.L. (1968): Empirical correction factors for the electron microanalysis of silicates and oxides. *J. Geol.*, **76**, 382–403.
- BRADY, J.B. and McCALLISTER, R.H. (1983): Diffusion data for clinopyroxenes from homogenization and self-diffusion experiments. *Am. Mineral.*, **68**, 95–105.
- BUSECK, P.R. and CLARK, J. (1984): Zaisho - a pallasite containing pyroxene and phosphoran olivine. *Mineral. Mag.*, **48**, 229–235.
- CASANOVA, I., GRAF, T. and MARTI, K. (1995): Discovery of an unmelted H-chondrite inclusion in an iron meteorite. *Science*, **268**, 540–542.
- CHRISTOFFERSEN, R., YUND, R.A. and TULLIS, J. (1983): Inter-diffusion of K and Na in alkali feldspars: Diffusion couple experiments. *Am. Mineral.*, **68**, 1126–1133.
- EVENSEN, N.M., HAMILTON, P.J., HARLOW, G.E., KLIMENTIDIS, R., O'NIONS, R.K. and PRINZ, M. (1979): Silicate inclusions in Weekeroo Station: Planetary differentiates in an iron meteorite. *Lunar and Planetary Science X*. Houston, Lunar Planet Inst., 376–378.
- GROSSMAN, L. (1972): Condensation in the primitive solar nebula. *Geochim. Cosmochim. Acta*, **36**, 597–619.
- HAGGERTY, S.E. (1973): Armalcolite and genetically associated opaque minerals in the lunar samples. *Proc. Lunar Sci. Conf.*, 4th, Vol. 1, 777–797.
- HARAMURA, H., KUSHIRO, I. and YANAI, K. (1983) Chemical compositions of Antarctic meteorites I. *Mem. Natl Inst. Polar Res., Spec Issue*, **30**, 109–121.
- ISHII, T. (1975): The relations between temperature and composition of pigeonite in some lavas and their application to geothermometry. *Mineral. J.*, **8**, 48–57.
- JAROSEWICH, E. (1990): Chemical analyses of meteorites: A compilation of stony and iron analyses. *Meteoritics*, **25**, 323–337.
- LINDSLEY, D.H. and ANDERSEN, D.J. (1983): A two-pyroxene thermometer. *Proc. Lunar Planet. Sci., Conf.*, 13th, Pt. 2, A887–A906 (*J. Geophys. Res.*, **88** Suppl.).
- MAYEDA, T.K. and CLAYTON, R.N. (1989): Oxygen isotopic compositions of unique Antarctic meteorites. *Papers Presented to the 14th Symposium on Antarctic Meteorites, June 6–8, 1989*. Tokyo, Natl Inst. Polar Res., 172.
- MCCOY, T.J. (1995): Silicate-bearing IIE irons: Early mixing and differentiation in a core-mantle environment and shock resetting of ages. *Meteoritics*, **30**, 542–543.
- MUELLER, R.F. and SAXENA, S.K. (1977): *Chemical Petrology*. New York, Springer.
- MUKHERJEE, A.B., BULATOV, V. and KOTELNIKOV, O.O., (1990): New high P-T experimental results on orthopyroxene-chrome spinel equilibrium and a revised orthopyroxene-spinel cosmo-thermometer. *Proc. Lunar Planet. Sci. Conf.*, 20th, 299–308.
- OLSEN, E. and JAROSEWICH, E. (1971): Chondrules: First occurrence in an iron meteorite. *Science*, **174**, 583–585.
- OLSEN, E., DAVIS, A., CLARKE, R.S., SCHULTZ, L., WEBER, H.W., CLAYTON, R., MAYEDA, T., JAROSEWICH, E., SYLVESTER, P., GROSSMAN, L., WANG, M.S., LIPSCHUTZ, M.E., STEELE, I.M. and SCHWADE, J. (1994): Watson: A new link in the IIE iron chain. *Meteoritics*, **29**, 200–213.
- REUTER, K.B., WILLIAMS, D.B. and GOLDSTEIN, J.I. (1989): Determination of the Fe-Ni phase diagram below 400°C. *Metall. Trans.*, **20A**, 719–725.
- RINGWOOD, A.E. (1979): *Origin of the Earth and Moon*. New York, Springer, 295p.
- ROBIE, R.A., HEMINGWAY, B.S. and FISHER, J.R. (1979): Thermodynamic properties of minerals and related substances at 298.15 K and 1 bar (10⁵ Pascals) pressure and at higher temperatures. *U. S. Geol. Surv. Bull.*, **1452**, 456p.
- ROMIG, A.D., Jr. and GOLDSTEIN, J.I. (1980): Determination of the Fe-Ni and Fe-Ni-P phase diagrams at low temperatures (700 to 300°C). *Metall. Trans.*, **11A**, 1151–1159.
- RUBIN, A.E., JERDE, E.A., ZONG, P., WASSON, J.T., WESTCOTT, J.W., MAYEDA, T.K. and CLAYTON, R.N. (1986):

- Properties of the Guin ungrouped iron meteorite: the origin of Guin and of group-IIE irons. *Earth Planet. Sci. Lett.*, **76**, 209–226.
- SCHAIER, J.F. (1950): The alkali-feldspar join in the system $\text{NaAlSi}_3\text{O}_8$ - KAlSi_3O_8 - SiO_2 . *J. Geol.*, **58**, 512–518.
- STORMER, J.C., Jr. and WHITNEY, J.A. (1977): Two-feldspar geothermometry in granulite facies metamorphic rocks. *Contrib. Mineral. Petrol.*, **65**, 123–133.
- TUTTLE, O.F. and BOWEN, N.L. (1958): Origin of granite in the light of experimental studies in the system $\text{NaAlSi}_3\text{O}_8$ - KAlSi_3O_8 - SiO_2 - H_2O . *Geol. Soc. Am. Mem.*, **74**, 000p.
- WASSON, J.T. and WANG, J. (1986): A nonmagmatic origin of group-IIE iron meteorites. *Geochim. Cosmochim. Acta*, **50**, 725–732.
- WILLIAMS, R.J. (1971): Equilibrium temperatures, pressures, and oxygen fugacities of the equilibrated chondrites. *Geochim. Cosmochim. Acta*, **35**, 407–411.
- WLOTZKA, F. (1994): *Meteoritical Bulletin 77*. *Meteoritics*, **29**, 893.
- YODER, H.S., Jr. and TILLEY, C.E. (1962): Origin of basalt magmas and experimental study of natural and synthetic rock systems. *J. Petrol.*, **3**, 342–532.

(Received September 8, 1995; Revised manuscript accepted November 7, 1995)